$^{40}Ar/^{39}Ar$ geochronology data from the Big Delta, Charley River, Circle, Fairbanks, and Livengood quadrangles, Alaska

Travis J. Naibert, Florian Hofmann, and Rainer J. Newberry

Raw Data File 2026-21



Field photo of rocks from station 24Z154 in the Chena Project area.

Raw Data Files provide elevation data, field observations, or analytical data. They are reviewed for clarity and consistency but do not undergo technical peer review.

State of Alaska
Department of Natural Resource
Division of Geological & Geophysical Surveys

State of Alaska
Mike Dunleavy, Governor

Department of Natural Resources
John Crowther, Commissioner

Division of Geological & Geophysical Surveys
Erin A. Campbell, State Geologist & Director

Publications produced by the Division of Geological & Geophysical Surveys are available to download from the DGGS website (http://dggs.alaska.gov/). Publications on hard-copy or digital media can be examined or purchased in the Fairbanks office:

Alaska Division of Geological & Geophysical Surveys (DGGS)
3354 College Road | Fairbanks, Alaska 99709-3707
Phone: 907.451.5010 | Fax 907.451.5050
dggspubs@alaska.gov

DGGS publications are also available at:
Alaska State Library
Historical Collections & Talking Book Center
395 Whittier Street
Juneau, Alaska 99801

Alaska Resource Library and Information Services (ARLIS)
Library Building, Suite 111
3211 Providence Drive
Anchorage, AK 99508

Suggested citation:
Naibert, T.J., Hofmann, Florian, and Newberry, R.J., 2026, 40Ar/39Ar geochronology data from the Big Delta, Charley River, Circle, Fairbanks, and Livengood quadrangles, Alaska: Alaska Division of Geological & Geophysical Surveys Raw Data File 2026-21, 36 p. https://doi.org/10.14509/32139

$^{40}Ar/^{39}Ar$ geochronology data from the Big Delta, Charley River, Circle, Fairbanks, and Livengood quadrangles, Alaska

Travis J. Naibert[1], Florian Hofmann[2], and Rainer J. Newberry[1]

INTRODUCTION

During the 2024 field season, geologists from the Alaska Division of Geological & Geophysical Surveys (DGGS) conducted 1:100,000-scale geologic mapping for the Chena and Steese projects within the Big Delta, Circle, Charley River, Fairbanks, and Livengood 1:250,000 quadrangles (fig. 1). Mapping was funded by the U.S. Geological Survey (USGS) Earth Mapping Resources Initiative (Earth MRI) program and the State of Alaska with an aim of producing more detailed and modern geologic maps and supporting datasets to promote mineral resource exploration in Interior Alaska.

The Chena project includes the Chena and Salcha River drainages as well as parts of the Birch Creek and Goodpaster River drainages. The Chena project area also includes the Pogo gold mine and surrounding exploration projects. The Steese project includes the Fairbanks area, the areas adjacent to the Steese Highway between the communities of Fairbanks and Central, and the White Mountains National Recreation Area and adjacent state lands to the east. Mineral systems in the region are orogenic (including the Pogo mine) and reduced intrusion-related systems involving mid-Cretaceous plutons (Hofstra and Kreiner, 2020). Furthermore, the Steese project area includes the Fairbanks and the Circle mining districts and contains many current and historic placer gold mining operations. The Chena and Steese map areas have potential to host critical minerals including rare earth elements, Sn, W, Te, Bi, Sb, As, F, and U.

The 26 $^{40}Ar/^{39}Ar$ analyses reported here are from 21 samples collected within the boundaries of the Chena and Steese projects (fig. 1). We collected geochronology samples to provide quantitative age control to help distinguish units with similar field appearance, resolve the timing of tectonic and magmatic events, and strengthen correlations across the map area. Age data for magma crystallization, metamorphism, and exhumation will further our knowledge of the magmatic and orogenic mineral systems in the region. Samples will be stored at DGGS for the duration of the projects and, upon project completion, will be transferred to the Alaska Geologic Materials Center in Anchorage. Samples will be available for public viewing upon request. These data and accompanying discussion are released as a DGGS Raw Data File, and all publication components are available from the DGGS website at https://doi.org/10.14509/32139.

DATA PRODUCTS

- Summary data spreadsheet and accompanying data dictionary
- Analytical lab data and accompanying data dictionary

[1] Alaska Division of Geological & Geophysical Surveys, 3354 College Road, Fairbanks, AK 99709
[2] Geochronology Laboratory, Reichardt 369, University of Alaska Fairbanks, 1930 Yukon Dr., Fairbanks, AK 99775

METHODS

Sample Collection

DGGS field geologists collected relatively unweathered samples from surface outcrops and selected them for age dating based on terrane, map unit, and the abundance of viable mineral phases. Samples were studied as hand specimens under a binocular microscope, and most samples were also studied in thin section under a petrographic microscope to identify unaltered target mineral phases for $^{40}Ar/^{39}Ar$ analyses.

Location data for samples were recorded in the WGS84 datum using GPS-enabled field tablets and are provided here in the NAD83 datum. Sample location coordinates have a typical reported accuracy of ±10 meters. The locations of the 21 samples presented in this report are shown in figure 1.

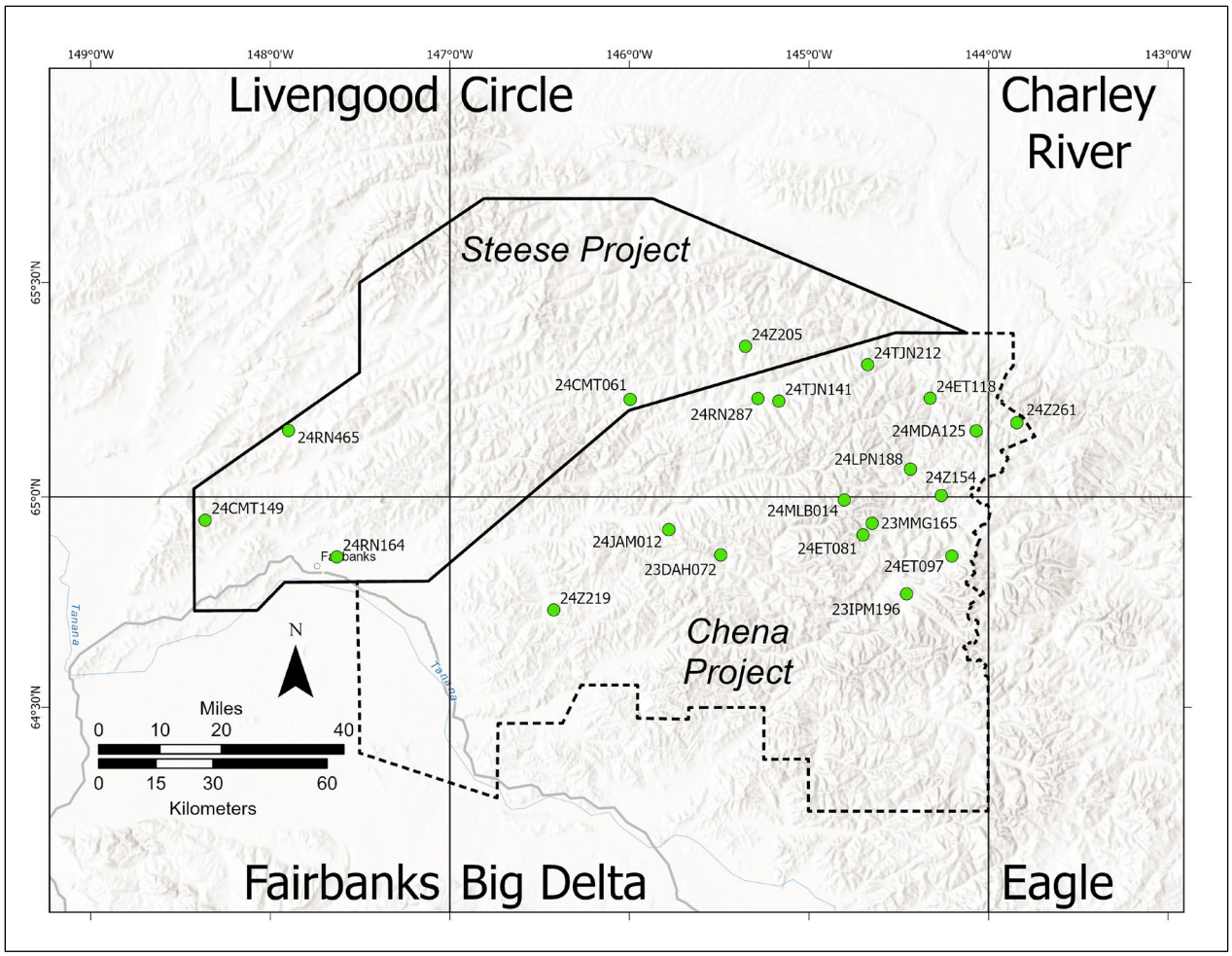

Figure 1. Location of samples analyzed for this report (green circles) within the Steese Project area (solid outline) and the Chena Project area (dashed outline). Large labels are 1:250,000 quadrangle names.

Sample Preparation

Rock samples were submitted to the Geochronology Laboratory at the University of Alaska Fairbanks (UAF) Geophysical Institute. Samples were crushed using jaw crushers and a

disk mill, and the crushed material was sieved to a grain size range of 250-500 μm. Target minerals were separated using a combination of magnetic separation with a Frantz isodynamic magnetic separator and density separation using sodium polytungstate (SPT). Suitable grains were picked with forceps under a light microscope to yield clean, homogeneous separates. Mica separates were cleaned by sonicating them in deionized water (DI) for 15 minutes and rinsing with DI until the water ran clear, followed by drying in a vacuum oven at 60 °C for 12 hours. The resulting cleaned mica samples were re-sieved to 250-500 μm and re-picked to remove any additional non-mica material revealed by the acid treatment.

About 20 mg of each final separate was wrapped in aluminum foil and loaded into oriented aluminum disks. Crystals of the Fish Canyon Tuff (FCT-UAF) sanidine flux monitor were placed on top of every 3-4 wells. The samples were irradiated in the Cadmium-Lined In-Core Irradiation Tube (CLICIT) at Oregon State University's TRIGA Reactor for 6 hours.

Analytical Methods

Aliquots were then transferred to a copper planchette and degassed with a Teledyne Photon Machines Fusions CO_2 laser in steps between 0.5% and 18-22% of maximum power for 30 seconds per step with a 2.2 mm diameter spot size. The extracted gas was purified with a SAES CapaciTorr ZAO getter, two SAES GP50 getters (one at room temperature, one at ~350 °C), and a liquid-nitrogen-cooled stainless-steel trap for 180 s. The resulting gas was analyzed with an Isotopx NGX-600 noble gas mass spectrometer. All five isotopes of argon (^{36}Ar-^{40}Ar) were measured simultaneously for 800 seconds using Faraday cups with ATONA amplifiers. Detector intercalibration was performed using air standards with a known ^{40}Ar/^{36}Ar ratio of 298.56 (Lee and others, 2006). Regularly interspersed blank analyses were used to correct measured data, with blank levels averaging around 2.4×10^{-16} mol ^{40}Ar and 8.6×10^{-19} mol ^{36}Ar.

Sample descriptions are summarized using field notes reported by Moshrefzadeh and others (2025) and updated with textural descriptions and sample mineralogy identified in thin section using polarized light microscopy. Mineral percentages were visually estimated in thin section.

Data Reduction

Data reduction was done with Pychron software (Ross, 2019), with corrections applied for atmospheric argon contamination, irradiation effects, and flux calibration, using a Fish Canyon Tuff age of 28.201±0.046 Ma (Kuiper, Deino, and others, 2008; Kuiper, Toorenburgh, and others, 2025) and a ^{40}K decay constant of 5.464×10^{-10} yr^{-1} (Min and others, 2000). The results are reported according to Schaen and others (2020). The accompanying data include a summary of the 40Ar/39Ar results, with ages quoted at the ±2σ level. The accompanying data also include step-heating results, with ages quoted at the ±1σ level. Age spectra plots and inverse isochron plots for each sample are included in Appendix A. The integrated age is the age given by the total gas measured and is equivalent to a potassium-argon (K-Ar) age. Age spectra provide plateau ages if three or more consecutive gas fractions account for at least 50 percent of the total

gas release and are within two standard deviations of each other (Mean Square Weighted Deviation [MSWD] < 2.5). When spectra did not meet one or more criteria for a plateau age under the above definition (e.g., MSWD was too high), we calculated a weighted mean age over several heating steps. These ages are considered less reliable than a plateau age.

Age spectra were calculated assuming an initial $^{40}Ar/^{36}Ar$ ratio equivalent to the atmospheric value of 298.56 ± 0.31 (Lee and others, 2006). We tested this assumption by plotting an inverse isochron for each sample. In many cases, the y-intercept of the inverse isochron plot indicates an initial $^{40}Ar/^{36}Ar$ ratio significantly higher than atmospheric (i.e., excess argon). For these samples, we recalculated the age spectra using the $^{40}Ar/^{36}Ar$ ratio from the inverse isochron, as listed in the digital data summary table. The recalculated age spectra should yield step-heating ages close to the isochron age rather than anomalously old ages (Heaton and Koppers, 2019). If this criterion was met for a sample, we used the recalculated age spectrum to identify a plateau or weighted mean age.

We identify our preferred age for each sample, which is generally the plateau age if the above plateau definition is met. If a plateau is not obtained, the preferred age is either the weighted mean of heating steps that meet some but not all of the plateau criteria or the isochron age derived from the inverse isochron plot. Samples with preferred ages based on the recalculated age spectrum are noted in the sample descriptions below and in the summary data table. Note that some plateaus depicted in figures in Appendix A do not satisfy all necessary criteria and are correctly identified as weighted mean ages in the text and the summary table provided in the accompanying digital data package.

RESULTS AND SAMPLE DESCRIPTIONS

23DAH072 - Metagrit

23DAH072 is a phyllitic metasandstone (metagrit) mapped in the greenschist-facies Butte assemblage (Newberry and others, 2026). The protolith was a poorly sorted granule sandstone with quartz and feldspar clasts up to 3.5 mm in a finer-grained matrix. Mineralogy includes 50 percent quartz, 20 percent chlorite, 16 percent albite, 7 percent potassium feldspar, and 7 percent white mica (0.03 to 0.25 mm). A white mica separate was dated and yielded an integrated age of 363.67 ± 0.13 Ma. No plateau age could be calculated from the age spectrum (fig. A1). Multiple heating steps yielded K/Ca ratios less than 15, suggesting the separate was contaminated with a Ca-bearing mineral. The white mica age spectrum was recalculated by assuming a trapped $^{40}Ar/^{36}Ar$ ratio of 37868 as calculated from the inverse isochron. The recalculated age spectrum is hump-shaped and yielded a weighted mean age of **149.3 ± 15.2** Ma over 7 non-consecutive heating steps (fig. A2), which is the preferred age for this sample.

23IPM196 - Phyllite

23IPM196 is a feldspathic phyllite mapped in the greenschist-facies Butte assemblage (Naibert and others, 2026). The sample is grayish green, phyllitic to sucrosic, and crenulated, with grain size ranging from 0.1 to 1 mm. Mineralogy includes 50 percent quartz, 24 percent

albite, 13 percent chlorite, 10 percent white mica, 1 percent potassium feldspar, 1 percent calcite, and 1 percent ilmenite. A white mica separate was dated and yielded an integrated age of 123.48 ± 0.03 Ma. The age spectrum has a stair-stepping up pattern without a plateau (fig. A3). The white mica age spectrum was recalculated by assuming a trapped $^{40}Ar/^{36}Ar$ ratio of 5690 as calculated from the inverse isochron. The recalculated age spectrum is hump-shaped and yielded a plateau age of 79.4 ± 6.0 Ma (fig. A4). This recalculated spectrum plateau is significantly younger than the isochron age. Consequently, this sample has no preferred age. Cooling of the sample through the argon closure temperature of white mica likely occurred during the Cretaceous.

23MMG165 - Paragneiss

23MMG165 is a paragneiss mapped in the Lake George assemblage in the West Point Gneiss Dome (Naibert and others, 2026). The sample is banded gray and white with a granoblastic texture and grain size between 0.03 and 2 mm. Mineralogy includes 60 percent quartz, 18 percent plagioclase, 10 percent muscovite, 8 percent biotite, 3 percent chlorite, 1 percent sillimanite, and minor garnet and ilmenite. Biotite and garnet are both partly replaced by chlorite and muscovite, and plagioclase and sillimanite are partly replaced by randomly oriented, fine-grained white mica. A muscovite separate was dated and yielded an integrated age of 89.7 ± 0.1 Ma. The age spectrum is generally flat, but consecutive heating-step ages do not overlap enough at the 2σ level to meet the definition of a plateau (Fig. A5). The muscovite age spectrum was recalculated by assuming a trapped $^{40}Ar/^{36}Ar$ ratio of 517 as calculated from the inverse isochron. The recalculated age spectrum yielded a plateau age of **88.5 ± 0.3 Ma**, which is the preferred age of the sample (fig. A6). The age may record cooling of the sample through the closure temperature of muscovite or may reflect the age of retrograde alteration experienced by the sample.

24CMT061 - Phyllite

24CMT061 is a dark gray granular phyllite interpreted to be in the Preacher Creek assemblage. Mineralogy includes 50 percent quartz, 20 percent albite, 13 percent white mica (0.03 to 0.15 mm), 10 percent chlorite, 3 percent graphite, 2 percent iron oxide, 1 percent apatite, and 1 percent ilmenite. A white mica separate was dated and yielded an integrated age of 403.0 ± 0.8 Ma. No plateau age could be calculated from the age spectrum (fig. A7). Low K/Ca ratios (less than 10) for many heating steps suggest the separate was contaminated with a Ca-bearing mineral. The white mica age spectrum was recalculated by assuming a trapped $^{40}Ar/^{36}Ar$ ratio of 11374 as calculated from the inverse isochron. The recalculated age spectrum yielded a plateau age of **350.3 ± 35.8 Ma** (fig. A8), which is the preferred age and is interpreted to record cooling of the sample through the closure temperature of white mica.

24CMT149 - Phyllitic metasandstone

24CMT149 is a phyllitic metasandstone interpreted to be in the Preacher Creek assemblage near Murphy Dome. Foliation is weak in hand sample, but muscovite grains are

strongly aligned in thin section. Mineralogy includes 65 percent quartz, 23 percent albite, 10 percent white mica (0.05 to 0.15 mm), and 2 percent chlorite. A white mica separate was dated and yielded an integrated age of 100.8 ± 0.1 Ma. No plateau age could be calculated from the age spectrum (fig. A9). The white mica age spectrum was recalculated by assuming a trapped $^{40}Ar/^{36}Ar$ ratio of 797 as calculated from the inverse isochron. The recalculated age spectrum yielded a weighted mean age of **89.7 ± 4.6 Ma** (fig. A10), which is the preferred age.

24ET081 - Paragneiss

24ET081 is a sillimanite-garnet-biotite paragneiss mapped in the Fairbanks-Chena assemblage (Naibert and others, 2026). The sample is mottled dark brown and gray with a gneissic texture and grain size between 1 and 3 mm. Mineralogy includes: 56 percent quartz, 15 percent biotite, 13 percent plagioclase, 6 percent sillimanite, 5 percent garnet, 2 percent fine-grained white mica (< 0.1 mm), 1 percent muscovite up to 0.2 mm, 1 percent chlorite, and 1 percent ilmenite. Fine-grained white mica partly replaces sillimanite and plagioclase; chlorite partly replaces biotite and garnet. A muscovite (plus white mica?) separate was dated and yielded an integrated age of 73.76 ± 0.03 Ma. No plateau age could be calculated from the age spectrum (fig. A11). The muscovite age spectrum was recalculated by assuming a trapped $^{40}Ar/^{36}Ar$ ratio of 3343 as calculated from the inverse isochron. The recalculated age spectrum yielded a plateau age of 55 ± 5 Ma (fig. A12). There is no preferred age for this sample because 1) the isochron and associated trapped $^{40}Ar/^{36}Ar$ ratio have very high uncertainty (MSWD=1343), and 2) the plateau age from the recalculated spectrum is significantly younger than the isochron age.

24ET097 - Quartz schist

24ET097 is a feldspathic quartz schist mapped in the Butte assemblage (Naibert and others, 2026). The sample is pale tan and massive, with grain size up to 0.5 mm. Mineralogy includes: 65 percent quartz (10 percent as 1-2 mm porphyroclasts), 24 percent muscovite, 10 percent alkali feldspar (as porphyroclasts), and 1 percent chlorite. A muscovite separate was dated and yielded an integrated age of 91.18 ± 0.11 Ma and a plateau age of **92.5 ± 0.1 Ma** (fig. A13). The plateau age is the preferred age of the sample and is interpreted to record cooling through the muscovite closure temperature.

24ET118 - Schist

24ET118 is a biotite-quartz-plagioclase-garnet-muscovite schist mapped in the Fairbanks-Chena assemblage (Naibert and others, 2026). The sample is brownish tan with grain sizes up to 15 mm. Mineralogy includes 25 percent muscovite, 25 percent garnet, 20 percent plagioclase, 15 percent quartz, 13 percent partially chloritized biotite, 1 percent sericite (up to 0.1 mm as partial replacement of plagioclase), minor ilmenite, and trace tourmaline. A biotite separate was dated and yielded an integrated age of 65.60 ± 0.06 Ma and an isochron age of **65.1 ± 0.6 Ma**. A weighted mean age of 66.06 ± 0.05 Ma was also calculated from 9 non-consecutive heating steps (fig. A14). The isochron age is the preferred age and is interpreted to record cooling of the sample through the biotite closure temperature. A muscovite separate was also dated and

yielded an integrated age of 65.69 ± 0.04 Ma and a plateau age of **65.46 ± 0.04 Ma** (fig. A15). The plateau age is the preferred age and is interpreted to record cooling of the sample through the muscovite closure temperature.

24JAM012 - Phyllite

24JAM012 is a crenulated phyllite mapped in the Blackshell assemblage (Newberry and others, 2026). Mineralogy includes 32 percent white mica, 30 percent quartz, 27 percent chlorite, 10 percent albite, and 1 percent ilmenite. White mica and chlorite are commonly interlayered. A white mica separate was dated and yielded an integrated age of 166.91 ± 0.05 and a stair-stepping up age spectrum with no plateau (fig. A16). The white mica age spectrum was recalculated by assuming a trapped $^{40}Ar/^{36}Ar$ ratio of 35550 as calculated from the inverse isochron. The recalculated age spectrum yielded a plateau age of 68 ± 9 Ma (fig. A17). There is no preferred age for this sample because 1) the isochron and associated trapped $^{40}Ar/^{36}Ar$ ratio have very high uncertainty (MSWD=297), and 2) the plateau age from the recalculated spectrum is significantly younger than the isochron age. The sample likely cooled through the argon closure temperature of white mica during the Jurassic or Cretaceous.

24LPN188 - Schist

24LPN188 is a kyanite-garnet-muscovite-sillimanite-biotite schist mapped in the Lake George assemblage in the West Point Gneiss Dome near the faulted contact with the Fairbanks-Chena assemblage (Naibert and others, 2026). The sample is dark gray and strongly foliated, with porphyroblasts up to 7 mm. Mineralogy includes 38 percent biotite (slightly chloritized), 30 percent quartz, 7 percent plagioclase, 13 percent sillimanite, 10 percent muscovite, 1 percent garnet, and 1 percent kyanite. A muscovite separate was dated and yielded an integrated age of 94.85 ± 0.02 Ma and a hump-shaped age spectrum with no plateau (fig. A18). The muscovite age spectrum was recalculated by assuming a trapped $^{40}Ar/^{36}Ar$ ratio of 1512 as calculated from the inverse isochron. The recalculated age spectrum yielded a plateau age of 84 ± 3 Ma (fig A19). There is no preferred age for this sample because 1) the isochron and associated trapped $^{40}Ar/^{36}Ar$ ratio have very high uncertainty (MSWD=1970), and 2) the plateau age from the recalculated spectrum is significantly younger than the isochron age. The sample likely cooled through the argon closure temperature of muscovite during the Late Cretaceous (ca. 100 to 80 Ma).

24MDA125 - Schist

24MDA125 is a kyanite-garnet-staurolite-mica schist mapped in the Fairbanks-Chena assemblage (Naibert and others, 2026). The sample has porphyroblasts up to 20 mm. Mineralogy includes 28 percent quartz, 20 percent muscovite, 17 percent plagioclase, 15 percent biotite, 12 percent staurolite, 4 percent garnet, 2 percent kyanite, 1 percent ilmenite, and trace tourmaline and apatite. The sample shows no evidence of retrograde metamorphism, such as chlorite after garnet or biotite. A muscovite separate was dated and yielded an integrated age of 82.81 ± 0.07 Ma and a stair-stepping up age spectrum that yielded a weighted mean age of **83.7 ± 0.2 Ma** (fig.

A20). The weighted mean age is the preferred age and is interpreted to record cooling of the sample through the muscovite closure temperature24MDA125.

24MLB014 - Schist

24MLB014 is a muscovite-plagioclase-biotite-quartz schist mapped in the Lake George assemblage (Naibert and others, 2026). The sample is tan to light brown and mylonitic, with grain sizes of 0.1 to 1 mm. Mineralogy includes 45 percent quartz (recrystallized), 25 percent biotite, 18 percent plagioclase (porphyroblastic), 11 percent muscovite, and trace tourmaline and ilmenite. Fine-grained white mica occurs in aggregates that partly replace plagioclase and completely replace sillimanite(?). A biotite separate was dated and yielded an integrated age of 84.66 ± 0.06 Ma and a plateau age of **85.00 ± 0.05 Ma** (fig. A21)**.** The plateau age is the preferred age for the sample and is interpreted to record cooling through the biotite closure temperature. A muscovite separate was also dated and yielded an integrated age of 166.56 ± 0.23 Ma and a hump-shaped age spectrum with no plateau (fig. A22). The muscovite age spectrum was recalculated by assuming a trapped $^{40}Ar/^{36}Ar$ ratio of 7328 as calculated from the inverse isochron. The recalculated age spectrum is also hump-shaped with no plateau (fig. A23). No preferred age is identified for the muscovite separate. The complex age spectra may be caused by multiple generations of muscovite/white mica in the separate.

24RN164 - Graphitic quartzite

24RN164 is a graphitic quartzite mapped in the Birch Hill Sequence (Newberry and others, 1996) and is interpreted to be correlative with the Blackshell Assemblage in recent DGGS mapping (Twelker, 2026). The sample is black, flaggy, and phyllitic with grain size ranging from 0.05 to 0.1 mm. Mineralogy includes 85 percent quartz, 10 percent white mica, 3 percent albite, and 2 percent graphite. A white mica separate was dated and yielded an integrated age of 128.48 ± 0.21 Ma and a saddle-shaped age spectrum with a plateau age of 119.5 ± 0.2 Ma (fig A24). The white mica age spectrum was recalculated by assuming a trapped $^{40}Ar/^{36}Ar$ ratio of 884, as calculated from the inverse isochron. The recalculated age spectrum yielded a weighted mean age of **115.3 ± 0.5 Ma** (fig. A25), which is the preferred age of the sample and is interpreted to record cooling through the closure temperature of white mica.

24RN287 - Phyllitic metasandstone

24RN287 is a phyllitic metasandstone/metagrit mapped in the Preacher Creek assemblage (Newberry and others, 2026). The sample is orange and greenish-grey with bimodal grain size. Coarse porphyroclasts are up to 1.5 mm. Mineralogy includes 67 percent quartz, 12 percent albite, 15 percent white mica, 3 percent ankerite (partly replaced by iron oxide), 2 percent chlorite, and 1 percent iron oxide. Two white mica separates were dated. The first separate (24RN287#1) yielded an integrated age of 168.44 ± 0.03 Ma and an age spectrum with older initial heating steps followed by younger heating steps, with a stair-stepping up pattern and no plateau (fig. A26). More than half of the heating steps yielded K/Ca ratios less than 15, suggesting some contamination of the white mica separate by a Ca-bearing mineral. The age spectrum was

recalculated by assuming a trapped $^{40}Ar/^{36}Ar$ ratio of 3133 as calculated from the inverse isochron. The recalculated age spectrum has a stair-stepping-up shape with a weighted mean age of 165.6 ± 2.0 Ma with MSWD = 38.19 (fig. A27). Because the MSWD is high for the recalculated spectrum-weighted mean age, this mineral separate has no preferred age, but the sample likely cooled through the closure temperature of white mica around **ca. 170 to 160 Ma**. The second white mica separate (24RN287 #2) yielded an integrated age of 229.33 ± 0.06 Ma and a hump-shaped age spectrum without a plateau age (fig. A28). We recalculated the age spectrum assuming a trapped $^{40}Ar/^{36}Ar$ ratio of 531, as calculated from the inverse isochron. The recalculated age spectrum is not flat enough to yield a plateau age (fig. A29). No preferred age is identified for the second white mica separate from this sample.

24RN465 - Phyllite

24RN465 is a chlorite-bearing phyllite interpreted to be in the Preacher Creek assemblage. Mineralogy includes 75 percent white mica, 10 percent chlorite, 6 percent albite, 5 percent quartz, and 4 percent titanite. Two white mica separates were dated. The first separate (24RN465 #1) yielded an integrated age of 124.15 ± 0.07 Ma and a stair-stepping up age spectrum without a plateau (fig. A30). The age spectrum was recalculated by assuming a trapped $^{40}Ar/^{36}Ar$ ratio of 3027 as calculated from the inverse isochron. The recalculated age spectrum also has a stair-stepping-up pattern with no plateau (fig. A31). There is no preferred age for this white mica separate. A second separate (24RN465 #2) yielded an integrated age of 123.31 ± 0.04 and a stair-stepping-up age spectrum (fig. A32). We recalculated the age spectrum assuming a trapped $^{40}Ar/^{36}Ar$ ratio of 26423, as calculated from the inverse isochron. The recalculated spectrum yielded a weighted mean age of **107.7 ± 3.0 Ma** (fig. A33), which is the preferred age and is interpreted to record the cooling of the sample through the closure temperature of white mica.

24TJN141 - Gabbro

24TJN141 is an altered hornblende gabbro (Naibert and others, 2026) dike. The sample is green and white, phaneritic, with phenocrysts up to 25 mm. Mineralogy includes 40 percent hornblende, 25 percent clinozoisite, 10 percent relict plagioclase, 10 percent chlorite, 7 percent biotite, 5 percent sericite, 3 percent titanite (ilmenite pseudomorphs). Epidote and sericite almost completely replace plagioclase. Chlorite partly replaces hornblende and biotite. A hornblende separate was dated and yielded an integrated age of 146.84 ± 0.28 Ma. The age spectrum did not yield a plateau (fig. A34). We recalculated the age spectrum assuming a trapped $^{40}Ar/^{36}Ar$ ratio of 1411, as calculated from the inverse isochron. The recalculated age spectrum yielded a weighted mean age of **95.5 ± 4.3 Ma** (fig. A35), which is the preferred age for this sample and is interpreted as the post-crystallization cooling age for this dike.

24TJN212 - Calcareous quartz schist

24TJN212 is a partly retrograded calcareous quartz schist mapped in the Fairbanks-Chena assemblage (Naibert and others, 2026). The sample is beige to tan with a schistose texture. Mineralogy includes 70 percent quartz, 12 percent white mica, 9 percent albite, 3 percent biotite,

2 percent calcite, 1 percent chlorite (secondary after biotite), and 1 percent iron oxide. The albite likely replaced plagioclase. A white mica separate was dated and yielded an integrated age of 98.28 ± 0.03 Ma and a stair-stepping up age spectrum with no plateau (fig. A36). More than half the heating steps yielded K/Ca ratios less than 15, suggesting some contamination of the white mica separate by a Ca-bearing mineral. The muscovite age spectrum was recalculated by assuming a trapped $^{40}Ar/^{36}Ar$ ratio of 1420 as calculated from the inverse isochron. The recalculated age spectrum also has a stair-stepping-up pattern with no plateau (fig. A37). This sample has no preferred age.

24Z154 - Schist

24Z154 is a garnet-bearing quartz mica schist mapped in the Fairbanks-Chena assemblage (Naibert and others, 2026). The sample is strongly foliated with garnet porphyroblasts and rare white quartz veins, which are described as focusing localized mineral growth of porphyroblastic staurolite, tourmaline, and muscovite crystals up to 2 centimeters (not seen in thin section). Mineralogy includes 38 percent quartz, 15 percent plagioclase (partly altered to sericite), 19 percent muscovite up to 1.5 mm, 15 percent biotite, 8 percent garnet, 3 percent chlorite, trace tourmaline and ilmenite. Biotite and garnet are partly altered to chlorite. A muscovite separate was dated and yielded an integrated age of 96.52 ± 0.06 Ma and a plateau age of **96.4 ± 0.1 Ma** (fig. A38). The plateau age is the preferred age and is interpreted to record cooling of the sample through the muscovite closure temperature.

24Z205 - Schist

24Z205 is a schist interpreted as part of the Preacher Creek assemblage. Mineralogy includes 40 percent white mica, 20 percent albite (porphyroblasts up to 1.5 mm), 15 percent quartz, 15 percent chlorite, 6 percent alkali feldspar, 2 percent ilmenite, 1 percent apatite, 1 percent biotite, and trace graphite and tourmaline. A biotite separate was dated and yielded an integrated age of 113.35 ± 0.06 Ma and a weighted mean age of **114.5 ± 0.1 Ma** (fig A39)**.** The weighted mean age is the preferred age for the biotite separate and is interpreted to record cooling through the biotite closure temperature. A white mica separate was also dated and yielded an integrated age of 112.57 ± 0.07 Ma and a weighted mean age of 113.8 ± 0.4 Ma (fig. A40). The muscovite age spectrum was recalculated by assuming a trapped $^{40}Ar/^{36}Ar$ ratio of 858, as calculated from the inverse isochron. The recalculated age spectrum yielded a plateau age of **111.9 ± 0.4 Ma** (fig. A41), which is the preferred age for the white mica separate and is interpreted to record cooling of the sample through the closure temperature of white mica.

24Z219 - Metafelsite

24Z219 is a felsic metavolcanic rock mapped in the Butte assemblage (Barrera and others, 2026). The sample is light yellow to greenish gray, foliated, and includes gray quartz porphyroclasts up to 4 mm in a fine matrix. Mineralogy includes 40 percent alkali feldspar, 30 percent quartz, 18 percent sericite (replacing groundmass), 10 percent albite, and 2 percent chlorite. A muscovite (sericite) separate was dated and yielded an integrated age of 97.43 ± 0.05

Ma and a stair-stepping up age spectrum with a weighted mean age of 101.95 ± 0.08 Ma (fig. A42). The muscovite age spectrum was recalculated by assuming a trapped $^{40}Ar/^{36}Ar$ ratio of 1028 as calculated from the inverse isochron. The recalculated age spectrum yielded a stair-stepping-up pattern with a weighted mean age of **97.9 ± 0.4 Ma** (fig. A43)**,** which is the preferred age of the sample and is interpreted to record cooling of the sample through the closure temperature of muscovite/sericite.

24Z261 - Schist

24Z261is a garnet–staurolite–quartz–plagioclase–biotite–muscovite schist mapped in the Fairbanks-Chena assemblage (Naibert and others, 2026). The sample is greenish-brown with garnet and staurolite porphyroblasts up to 20 mm. Mineralogy includes 30 percent muscovite, 20 percent biotite, 15 percent plagioclase, 10 percent quartz, 13 percent staurolite, 10 percent garnet, 1 percent chlorite, and 1 percent ilmenite. Biotite and garnet are slightly altered to chlorite. A muscovite separate was dated and yielded an integrated age of 69.08 ± 0.04 Ma and a stair-stepping up age pattern (fig. A44). The muscovite age spectrum was recalculated by assuming a trapped $^{40}Ar/^{36}Ar$ ratio of 449 as calculated from the inverse isochron. The recalculated age spectrum yielded a weighted mean age of **68.0 ± 0.2 Ma** (Fig. A45), which is the preferred age for the sample and is interpreted to record cooling through the closure temperature of muscovite.

ACKNOWLEDGMENTS

This work was jointly funded by the State of Alaska and the U.S. Geological Survey through the Earth Mapping Resources Initiative (Earth MRI) program cooperative agreements G23AC00372 and G24AC00323. The views and conclusions contained in this document are those of the authors and should not be interpreted as representing the opinions or policies of the U.S. Geological Survey. Mention of trade names or commercial products does not constitute their endorsement by the U.S. Geological Survey.

REFERENCES

Barrera, M.L., Newberry, R.J., Twelker, Evan, Buchanan, J.W., and Naibert, T.J., 2026, Bedrock geologic map of the Yukon Training Area and lower Salcha River, Big Delta and Fairbanks quadrangles, Alaska, in Twelker, Evan, ed., Geologic investigation of the Chena-Pogo area, Interior Alaska: Alaska Division of Geological & Geophysical Surveys Preliminary Interpretive Report 2026-3D, 1 sheet, scale 1:100,000, https://doi.org/10.14509/32115.

Heaton, D.E., and Koppers, A.A.P., 2019, High-resolution 40Ar/39Ar geochronology of the Louisville Seamounts IODP Expedition 330 drill sites—Implications for the duration of hot spot-related volcanism and age progressions: Geochemistry, Geophysics, Geosystems, v. 20, no. 8, p. 4073–4102, https://doi.org/10.1029/2018GC007759.

Hofstra, A.H., and Kreiner, D.C., 2020, Systems-Deposits-Commodities-Critical Minerals Table for the Earth Mapping Resources Initiative (ver. 1.1, May 2021): U.S. Geological Survey Open-File Report 2020–1042, 26 p., https://doi.org/10.3133/ofr20201042.

Kuiper, K.F., Deino, A.L., Hilgen, F.J., Krijgsman, Wout, Renne, P.R., and Wijbrans, J.R., 2008, Synchronizing rock clocks of Earth history: Science, v. 320, no. 5875, p. 500–504, https://doi.org/10.1126/science.1154339.

Kuiper, K.F., Toorenburgh, Zoe, Wotzlaw, J.F., Zeeden, Christian, Sierro, F.J., Davies, J.H., Sahy, Diana, Condon, D.J., and Hilgen, F.J., 2026, Revisiting the age of the Fish Canyon sanidine dating standard: Palaeogeography, Palaeoclimatology, Palaeoecology, v. 682, article 113421, 14 p., https://doi.org/10.1016/j.palaeo.2025.113421.

Lee, J.Y., Marti, Kurt, Severinghaus, J.P., Kawamura, Kenji, Yoo, H.S., Lee, J.B., and Kim, J.S., 2006, A redetermination of the isotopic abundances of atmospheric Ar: Geochimica et Cosmochimica Acta, v. 70, no. 17, p. 4507–4512, https://doi.org/10.1016/j.gca.2006.06.1563.

Min, Kyoungwon, Mundil, Roland, Renne, P.R., and Ludwig, K.R., 2000, A test for systematic errors in 40Ar/39Ar geochronology through comparison with U/Pb analysis of a 1.1-Ga rhyolite: Geochimica et Cosmochimica Acta, v. 64, no. 1, p. 73–98, https://doi.org/10.1016/S0016-7037(99)00204-5.

Moshrefzadeh, J.A., Buchanan, J.W., Naibert, T.J., Twelker, Evan, Newberry, R.J., Szumigala, D.J., Barrera, M.L., Norwood, L.P., Acosta, M.D., and Regan, S.P., 2025, Field station locations and magnetic susceptibility data collected in 2024 for the Chena and Steese projects, Yukon-Tanana Uplands, Alaska: Alaska Division of Geological & Geophysical Surveys Raw Data File 2025-5, 5 p., https://doi.org/10.14509/31476.

Naibert, T.J., Buchanan, J.W., Wilson, K.R., Regan, Sean, Truskowski, C.M., Szumigala, D.J., and Norwood, L.P., 2026, Bedrock geologic map of the upper Salcha River, East Fork Chena, and Big Windy Creek areas, Big Delta and Circle quadrangles, Alaska, in Twelker, Evan, ed., Geologic investigation of the Chena-Pogo area, Interior Alaska: Alaska Division of Geological & Geophysical Surveys Preliminary Interpretive Report 2026-3C, 1 sheet, scale 1:100,000, https://doi.org/10.14509/32114.

Newberry, R.J., Bundtzen, T.K., Clautice, K.H., Combellick, R.A., Douglas, Tom, Laird, G.M., Liss, S.A., Pinney, D.S., Reifenstuhl, R.R., and Solie, D.N., 1996, Preliminary geologic map of the Fairbanks mining district, Alaska: Alaska Division of Geological & Geophysical Surveys Public Data File 96-16, 17 p., 2 sheets, scale 1:63,360, https://doi.org/10.14509/1740.

Newberry, R.J., Naibert, T.J., and Barrera, M.L., 2026, Bedrock geologic map of the Granite Tors and Chena Hot Springs areas, Circle and Big Delta quadrangles, Alaska, in Twelker, Evan, ed., Geologic investigation of the Chena-Pogo area, Interior Alaska: Alaska Division of Geological & Geophysical Surveys Preliminary Interpretive Report 2026-3B, 1 sheet, scale 1:100,000, https://doi.org/10.14509/32113.

Ross, Jake, 2019, NMGRL/pychron (ver. 18.2): Zenodo software release, https://doi.org/10.5281/zenodo.3237834.

Schaen, A.J., Jicha, B.R., Hodges, K.V., Vermeesch, Pieter, Stelten, M.E., Mercer, C.M., Phillips, David, Rivera, T.A., Jourdan, Fred, Matchan, E.L., Hemming, S.R., Morgan, L.E., Kelley, S.P., Cassata, W.S., Heizler, M.T., Vasconcelos, P.M., Benowitz, J.A., Koppers, A.A.P., Mark, D.F., Niespolo, E.M., Sprain, C.J., Hames, W.E., Kuiper, K.F., Turrin, B.D., Renne, P.R., Ross, Jake, Nomade, Sebastian, Guillou, Herve, Webb, L.E., Cohen, B.A., Calvert, A.T., Joyce, Nancy, Ganerød, Morgan, Wijbrans, Jan, Ishizuka, Osamu, He, Huaiyu, Ramirez, Adán, Pfänder, J.A., Lopez-Martínez, Margarita, Qiu, Huaning, and Singer, B.S., 2021, Interpreting and reporting 40Ar/39Ar geochronologic data: Geological Society of America Bulletin, v. 133, no. 3–4, p. 461–487, https://doi.org/10.1130/B35560.1.

Twelker, Evan, ed., 2026, Geologic investigation of the Chena-Pogo area, Interior Alaska: Alaska Division of Geological & Geophysical Surveys Preliminary Interpretive Report 2026-3, 1 p., https://doi.org/10.14509/32111.

APPENDIX A – AGE SPECTRA AND INVERSE ISOCHRON PLOTS

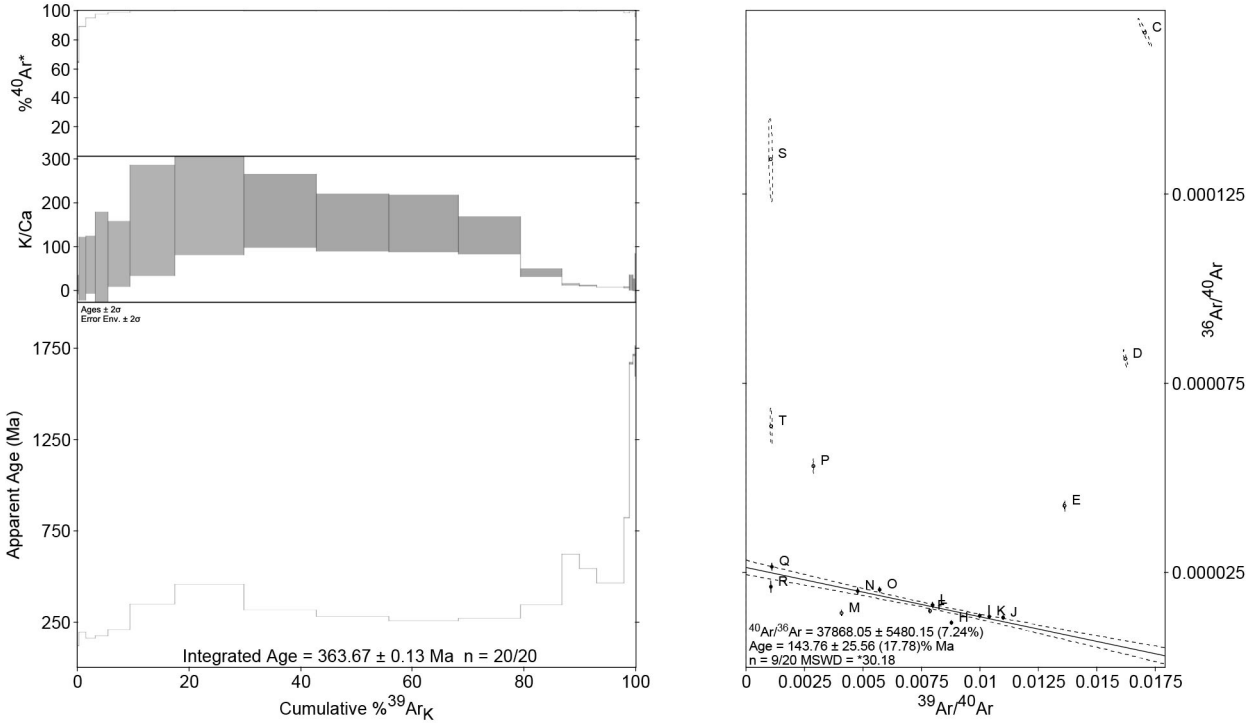

Figure A1. Age spectrum and inverse isochron plots for white mica sample 23DAH072.

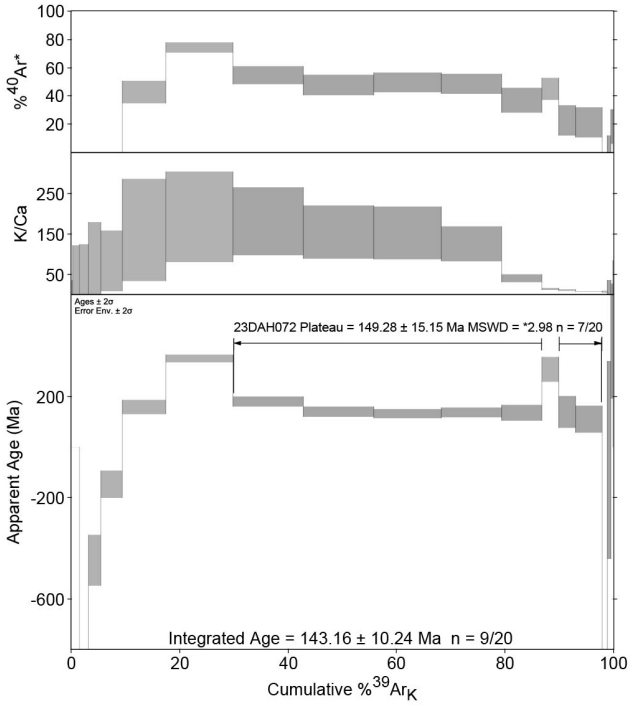

Figure A2. Recalculated age spectrum for white mica sample 23DAH072 using the initial $^{40}Ar/^{36}Ar$ ratio from the inverse isochron plot instead of the typical atmospheric $^{40}Ar/^{36}Ar$ ratio.

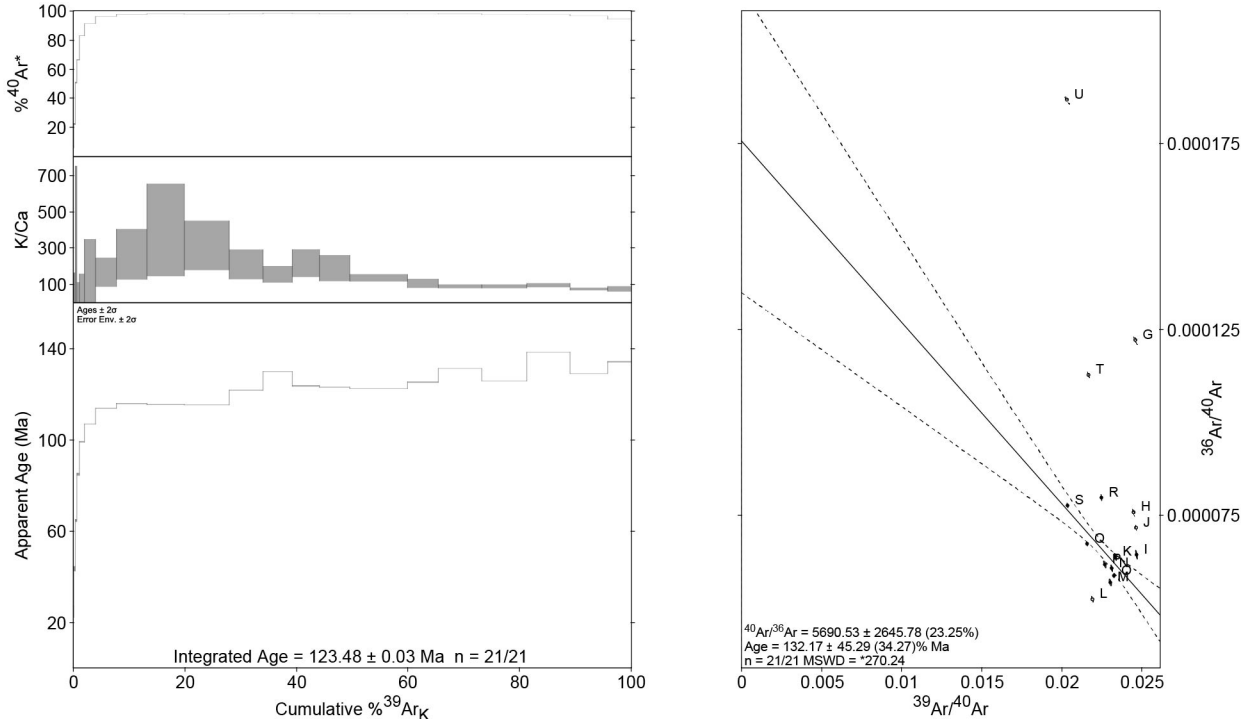

Figure A3. Age spectrum and inverse isochron plots for white mica sample 23IPM196.

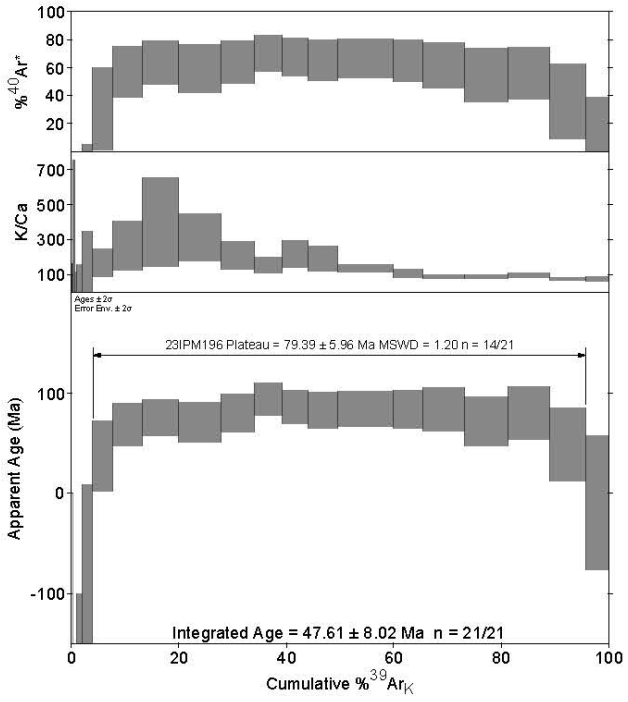

Figure A4. Recalculated age spectrum for white mica sample 23IPM196 using the initial $^{40}Ar/^{36}Ar$ ratio from the inverse isochron plot instead of the typical atmospheric $^{40}Ar/^{36}Ar$ ratio.

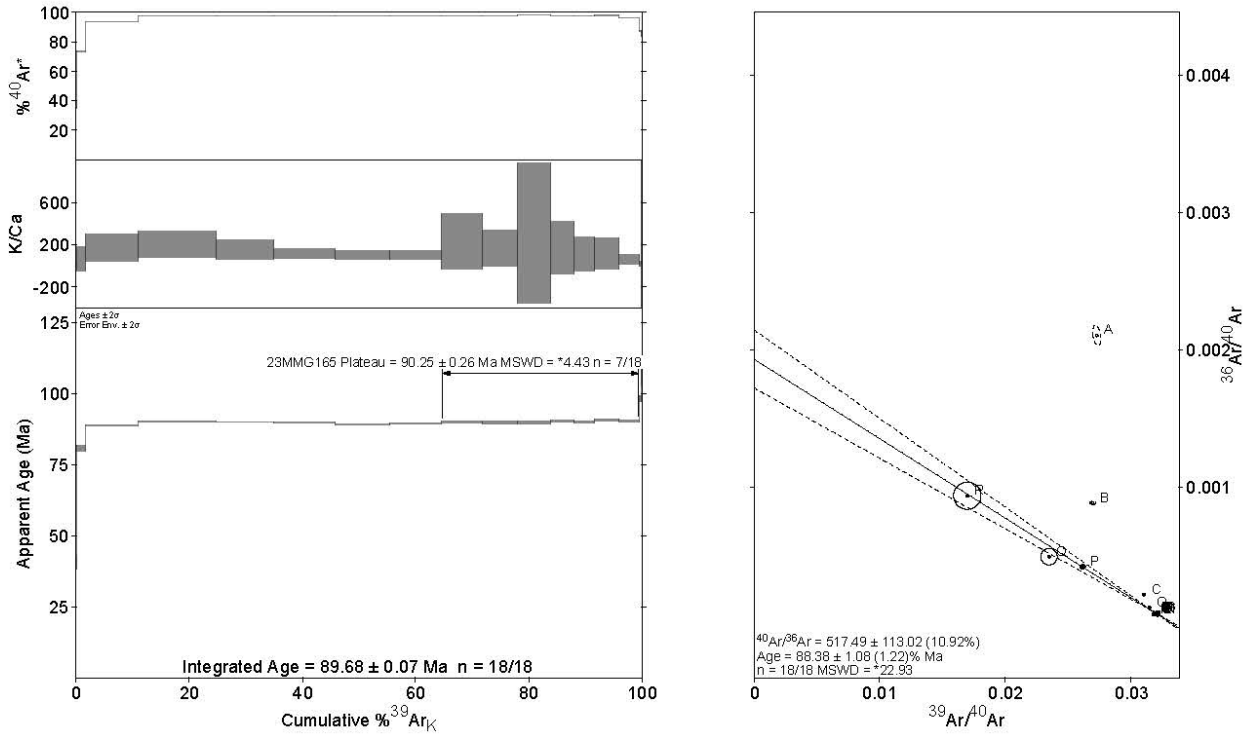

Figure A5. Age spectrum and inverse isochron plots for muscovite sample 23MMG165.

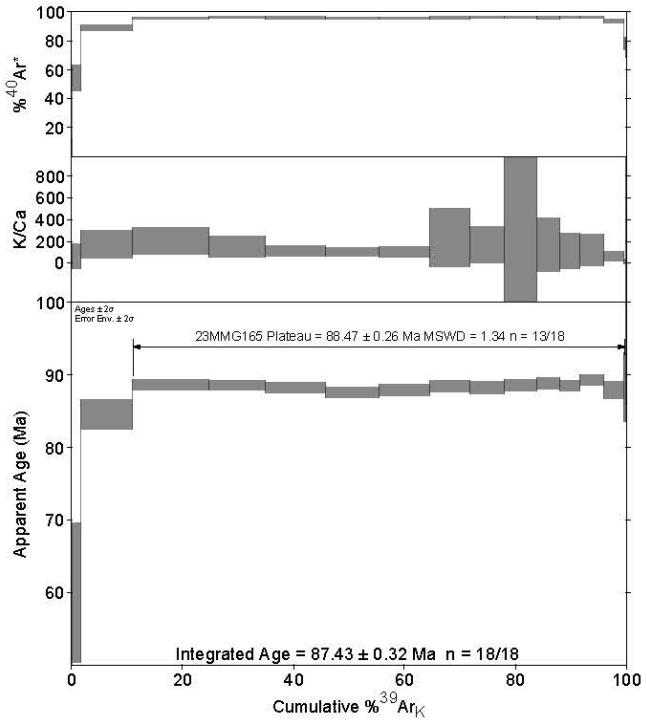

Figure A6. Recalculated age spectrum for muscovite sample 23MMG165 using the initial $^{40}Ar/^{36}Ar$ ratio from the inverse isochron plot instead of the typical atmospheric $^{40}Ar/^{36}Ar$ ratio.

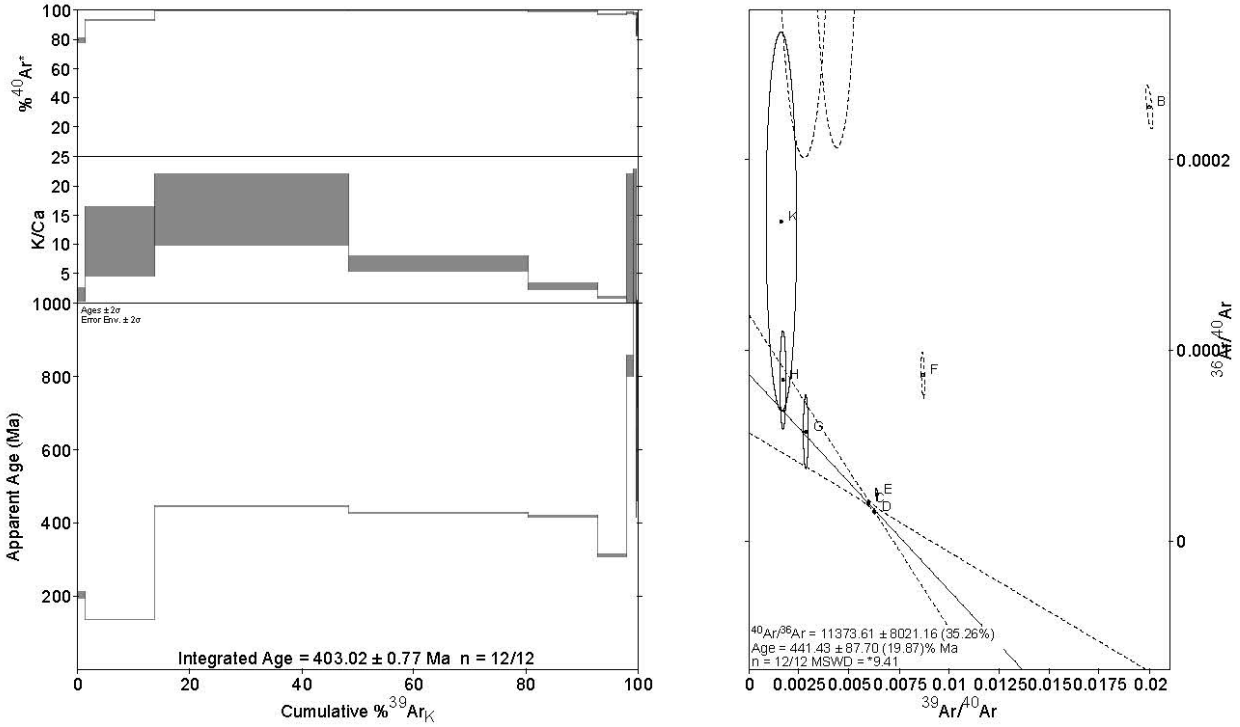

Figure A7. Age spectrum and inverse isochron plots for white mica sample 24CMT061.

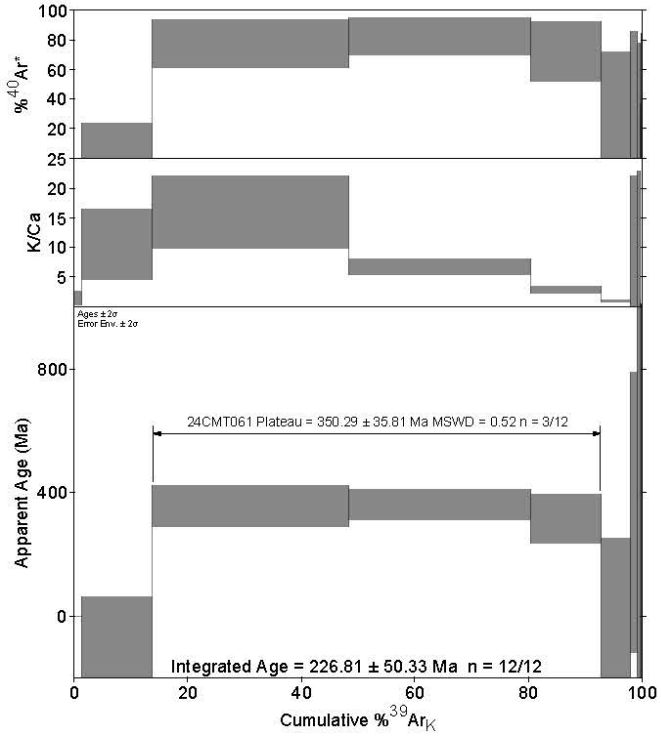

Figure A8. Recalculated age spectrum for white mica sample 24CMT061 using the initial $^{40}Ar/^{36}Ar$ ratio from the inverse isochron plot instead of the typical atmospheric $^{40}Ar/^{36}Ar$ ratio.

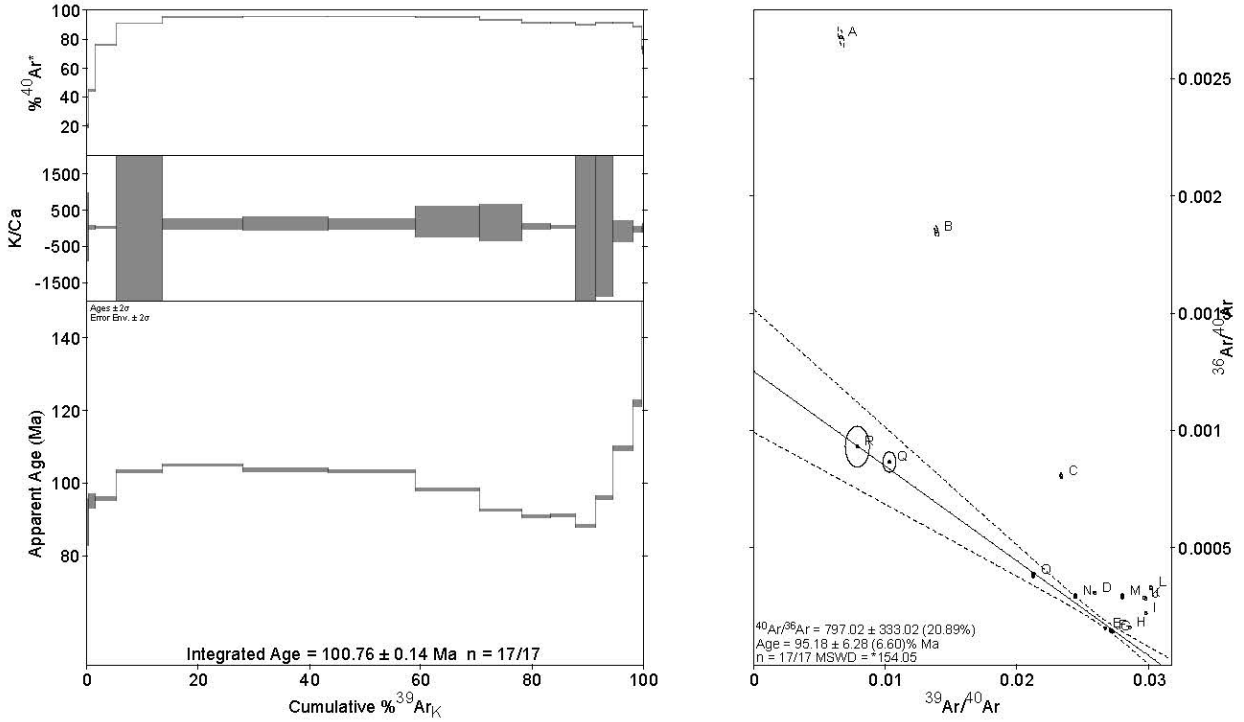

Figure A9. Age spectrum and inverse isochron plots for white mica sample 24CMT149.

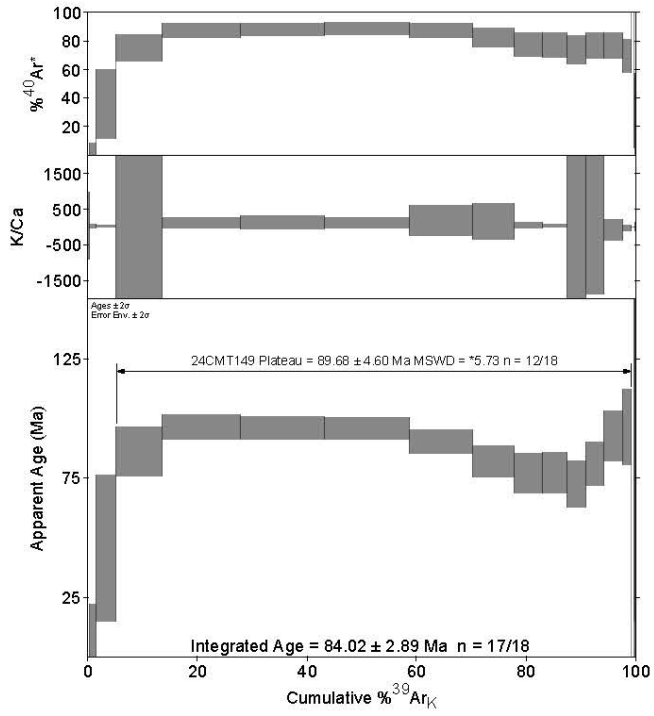

Figure A10. Recalculated age spectrum for white mica sample 24CMT149 using the initial $^{40}Ar/^{36}Ar$ ratio from the inverse isochron plot instead of the typical atmospheric $^{40}Ar/^{36}Ar$ ratio.

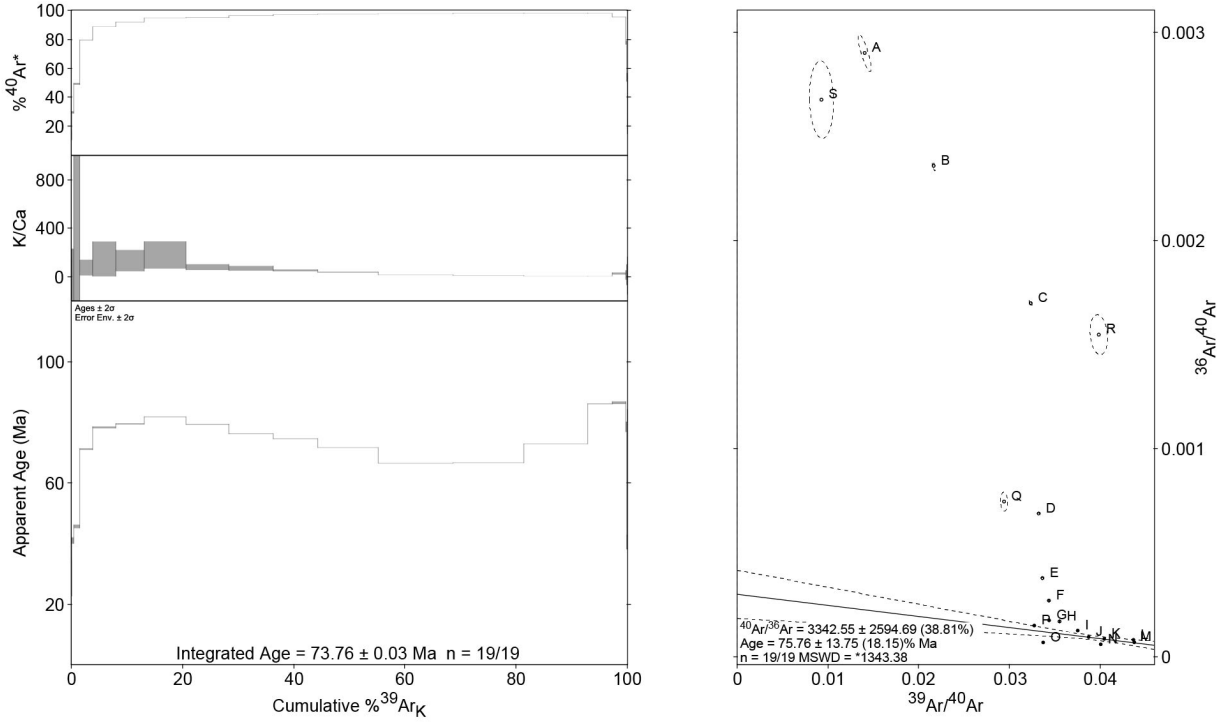

Figure A11. Age spectrum and inverse isochron plots for muscovite sample 24ET081.

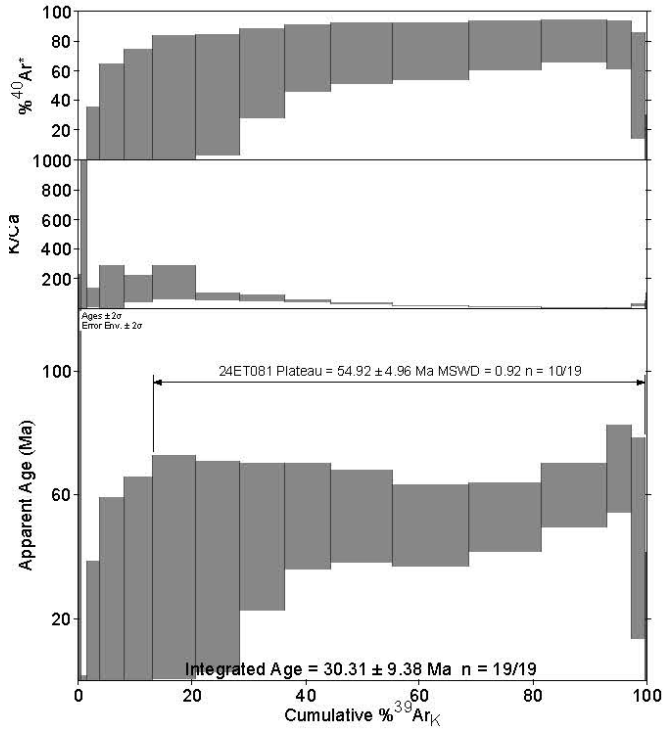

Figure A12. Recalculated age spectrum for muscovite sample 24ET081 using the initial $^{40}Ar/^{36}Ar$ ratio from the inverse isochron plot instead of the typical atmospheric $^{40}Ar/^{36}Ar$ ratio.

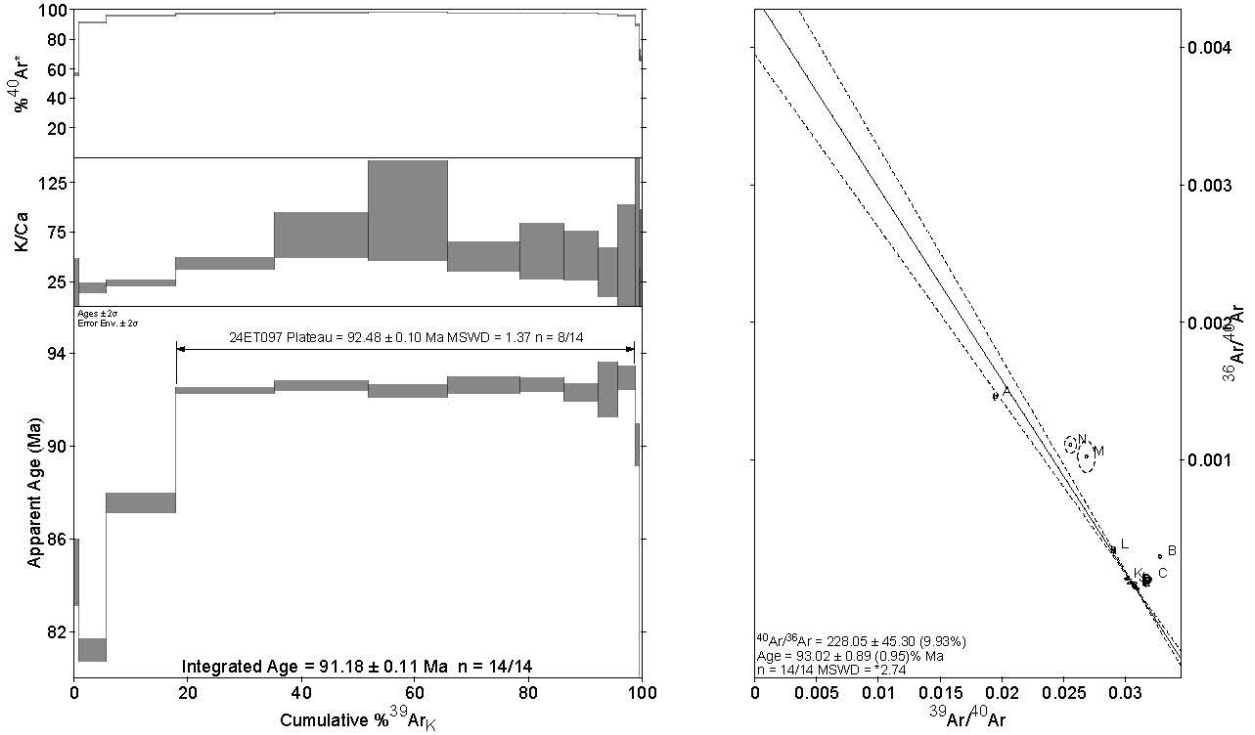

Figure A13. Age spectrum and inverse isochron plots for white mica sample 24ET097.

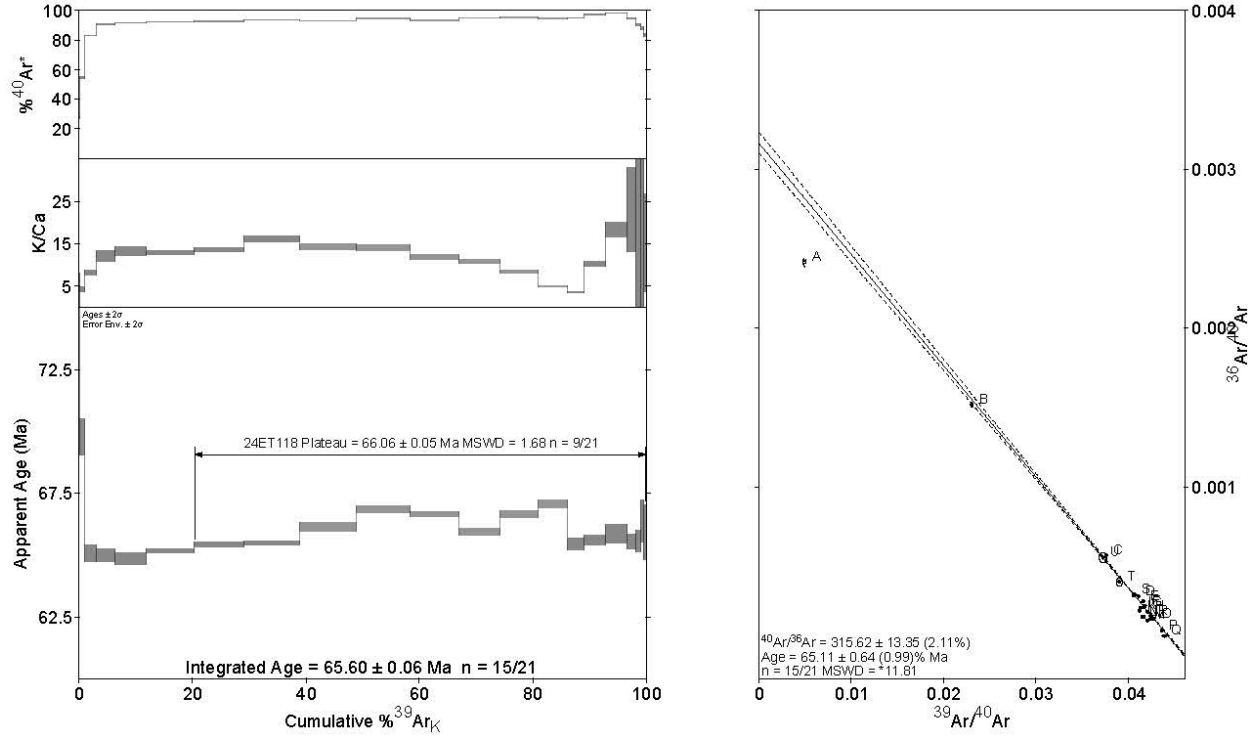

Figure A14. Age spectrum and inverse isochron plots for biotite sample 24ET118.

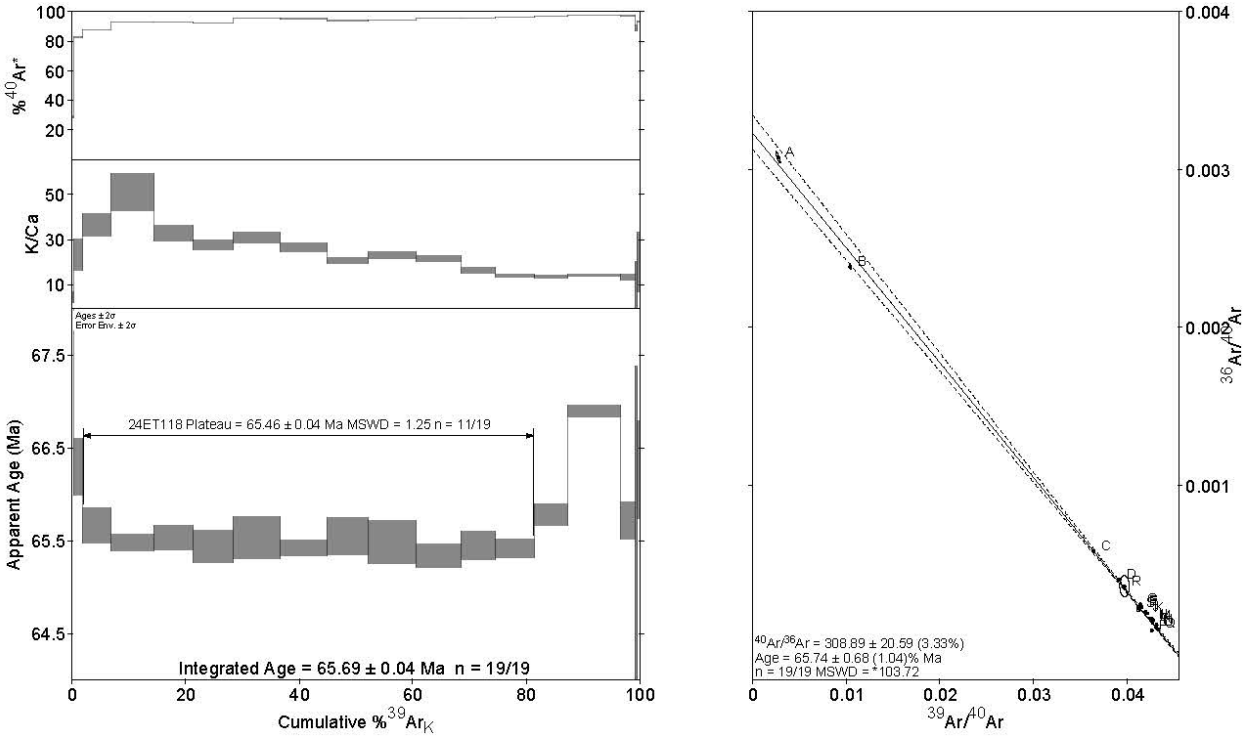

Figure A15. Age spectrum and inverse isochron plots for muscovite sample 24ET118.

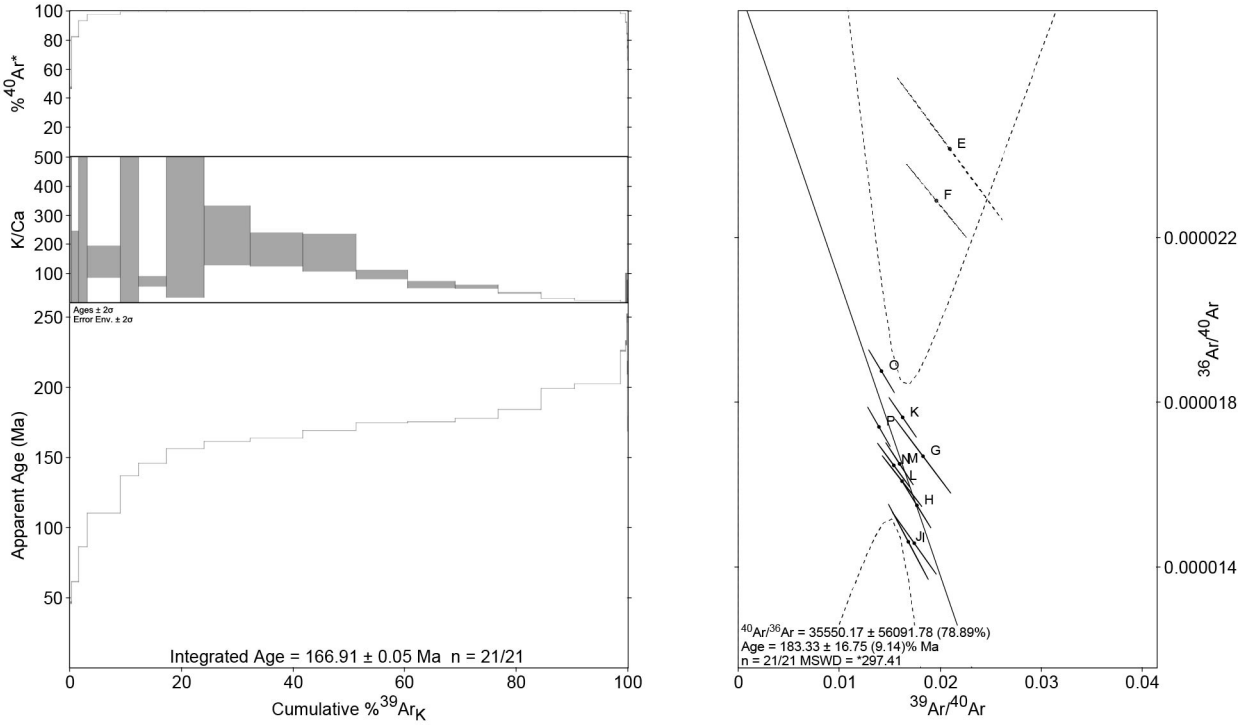

Figure A16. Age spectrum and inverse isochron plots for white mica sample 24JAM012.

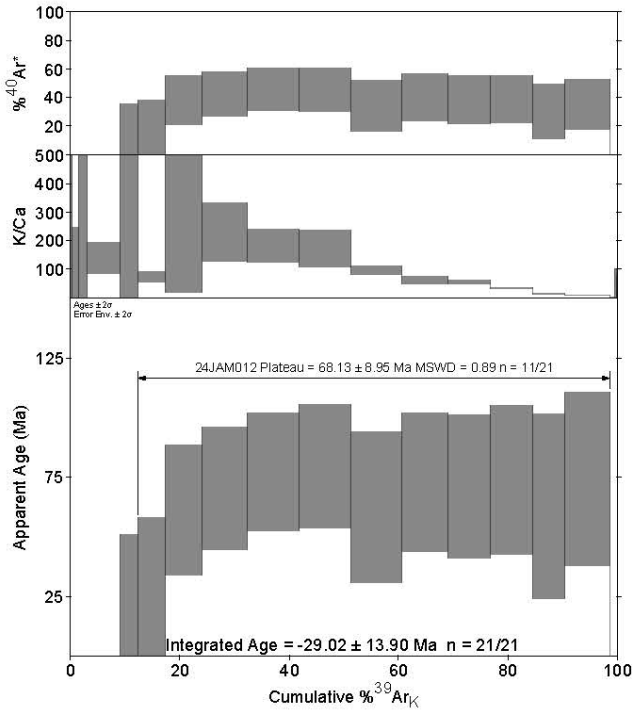

Figure A17. Recalculated age spectrum for white mica sample 24JAM012 using the initial 40Ar/36Ar ratio from the inverse isochron plot instead of the typical atmospheric 40Ar/36Ar ratio.

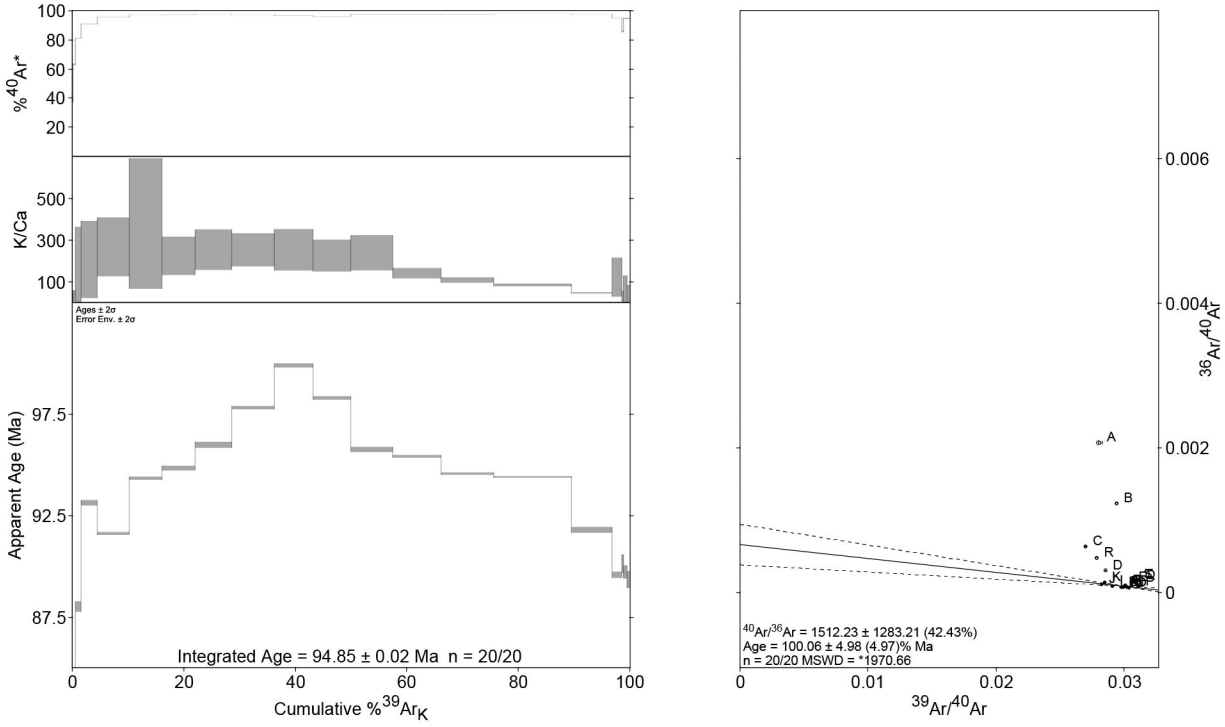

Figure A18. Age spectrum and inverse isochron plots for muscovite sample 24LPN188.

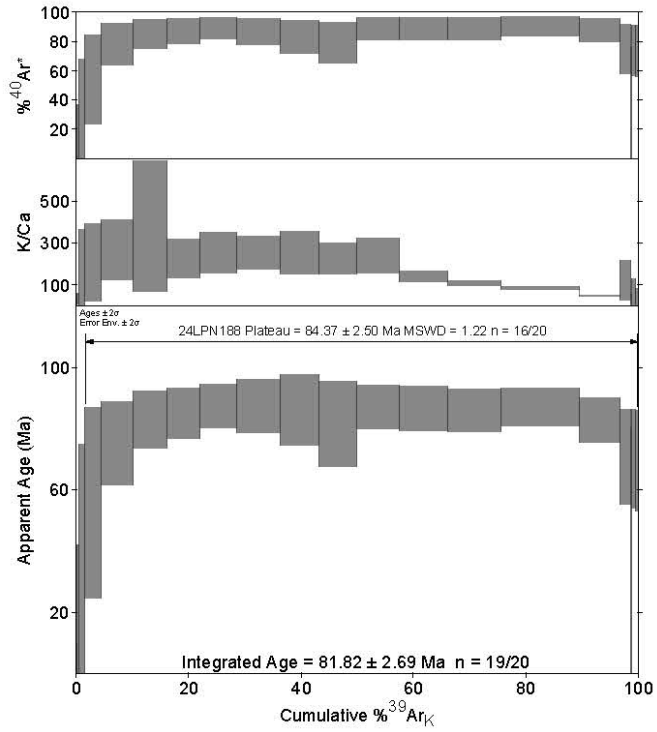

Figure A19. Recalculated age spectrum for muscovite sample 24LPN188 using the initial $^{40}Ar/^{36}Ar$ ratio from the inverse isochron plot instead of the typical atmospheric $^{40}Ar/^{36}Ar$ ratio.

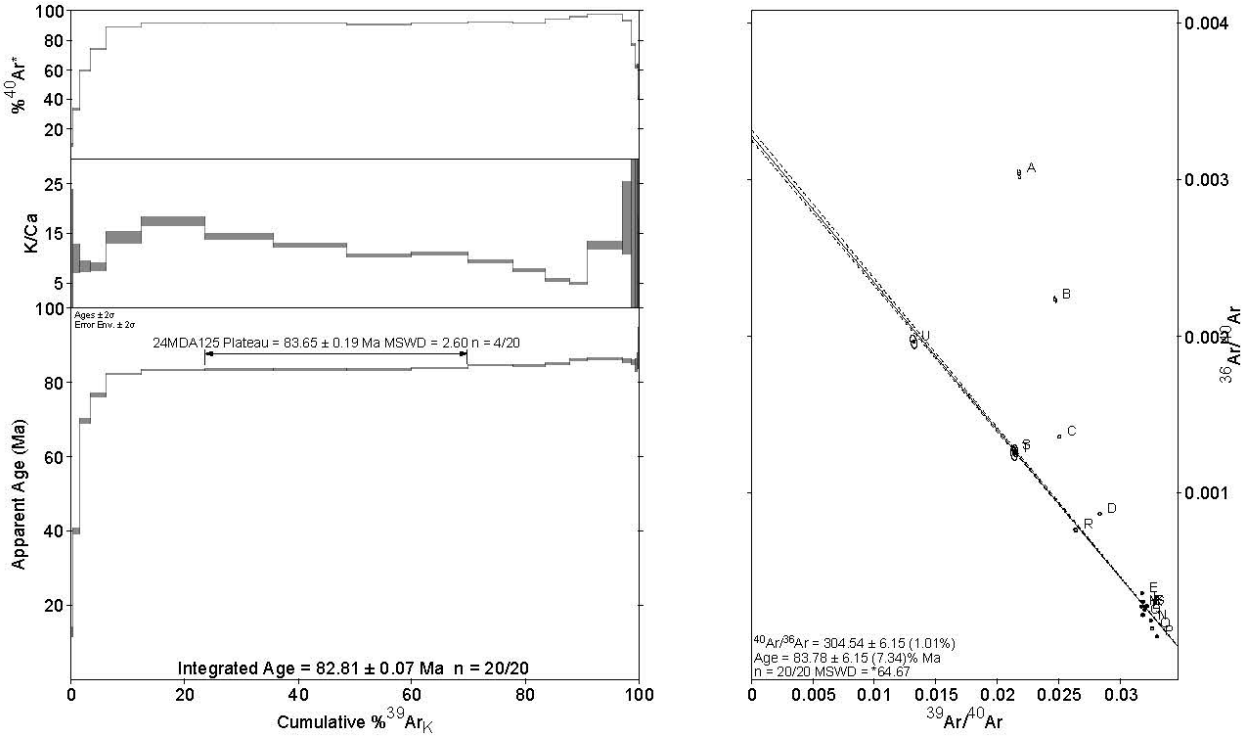

Figure A20. Age spectrum and inverse isochron plots for muscovite sample 24MDA125.

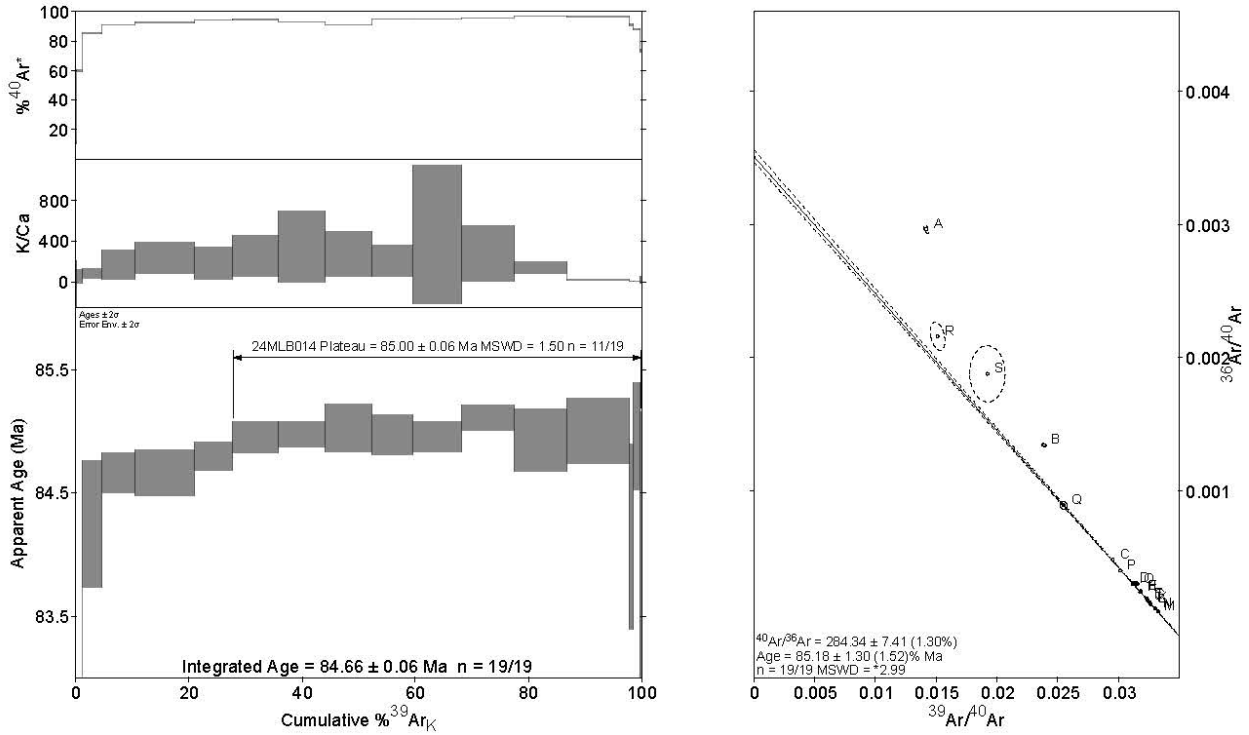

Figure A21. Age spectrum and inverse isochron plots for biotite sample 24MLB014.

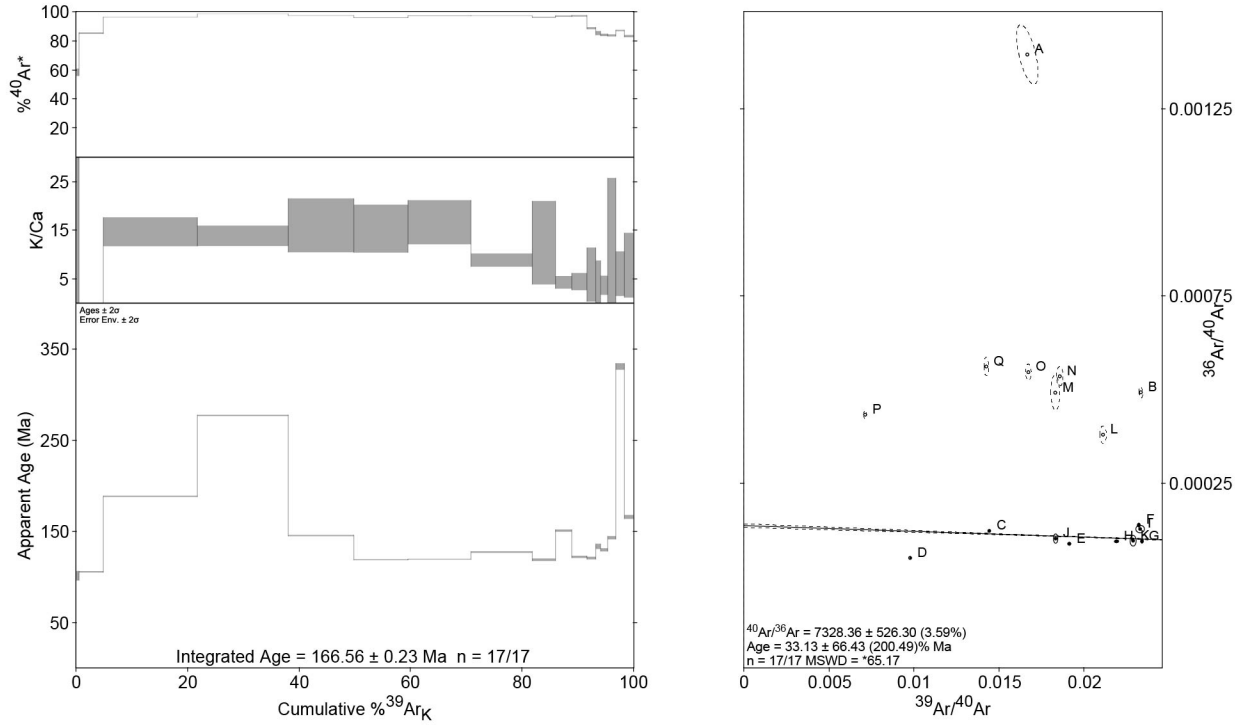

Figure A22. Age spectrum and inverse isochron plots for muscovite sample 24MLB014.

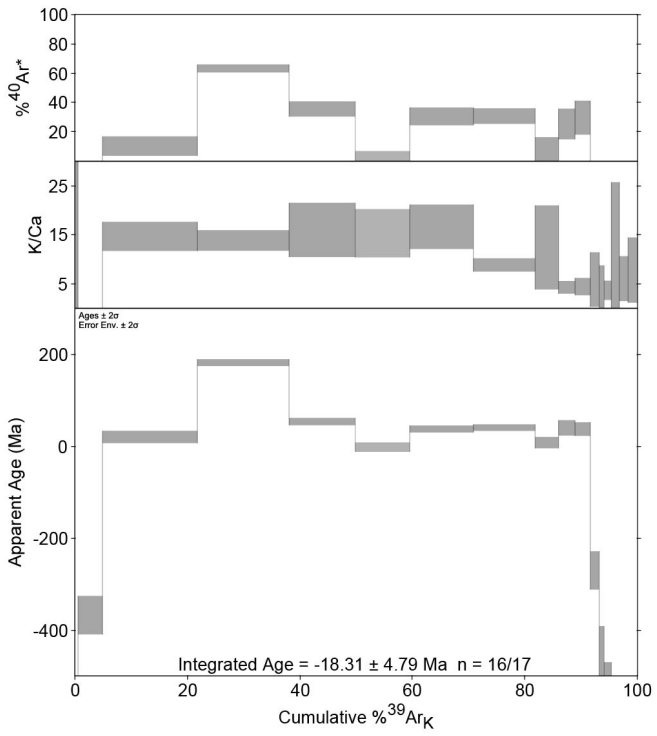

Figure A23. Recalculated age spectrum for muscovite sample 24MLB014 using the initial 40Ar/36Ar ratio from the inverse isochron plot instead of typical atmospheric 40Ar/36Ar ratio.

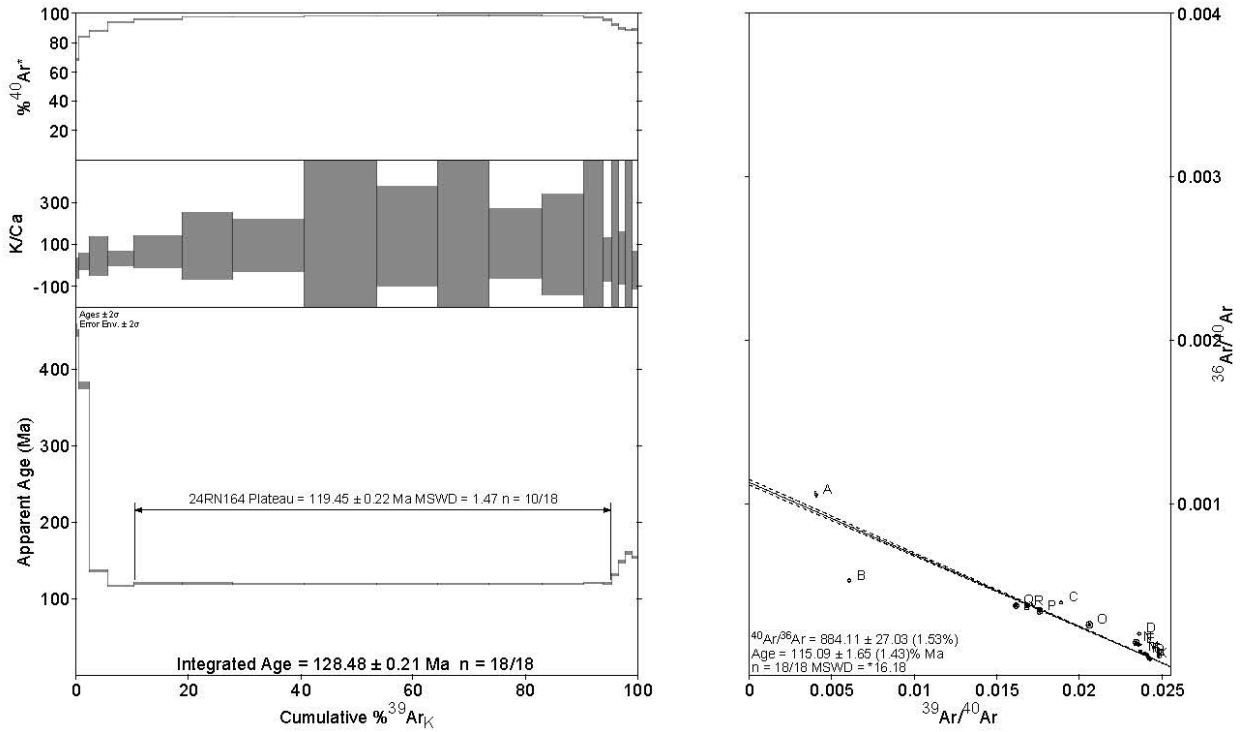

Figure A24. Age spectrum and inverse isochron plots for white mica sample 24RN164.

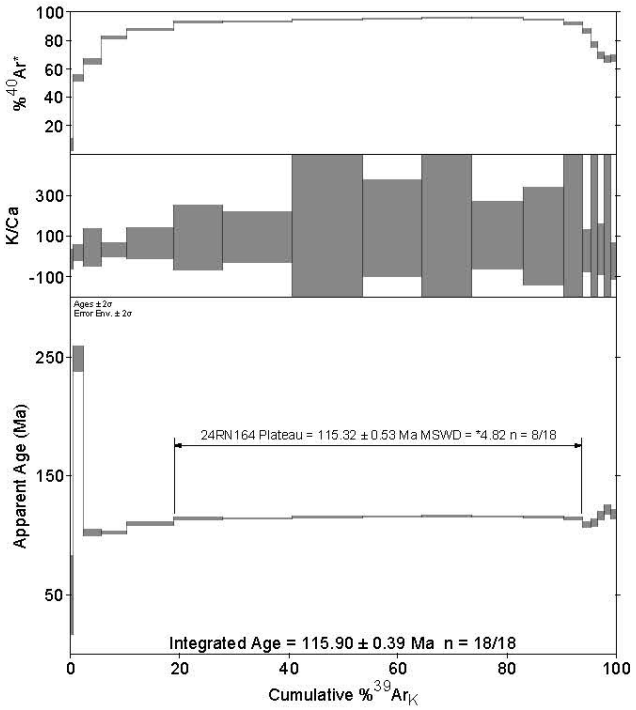

Figure A25. Recalculated age spectrum for white mica sample 24RN164 using the initial 40Ar/36Ar ratio from the inverse isochron plot instead of the typical atmospheric 40Ar/36Ar ratio.

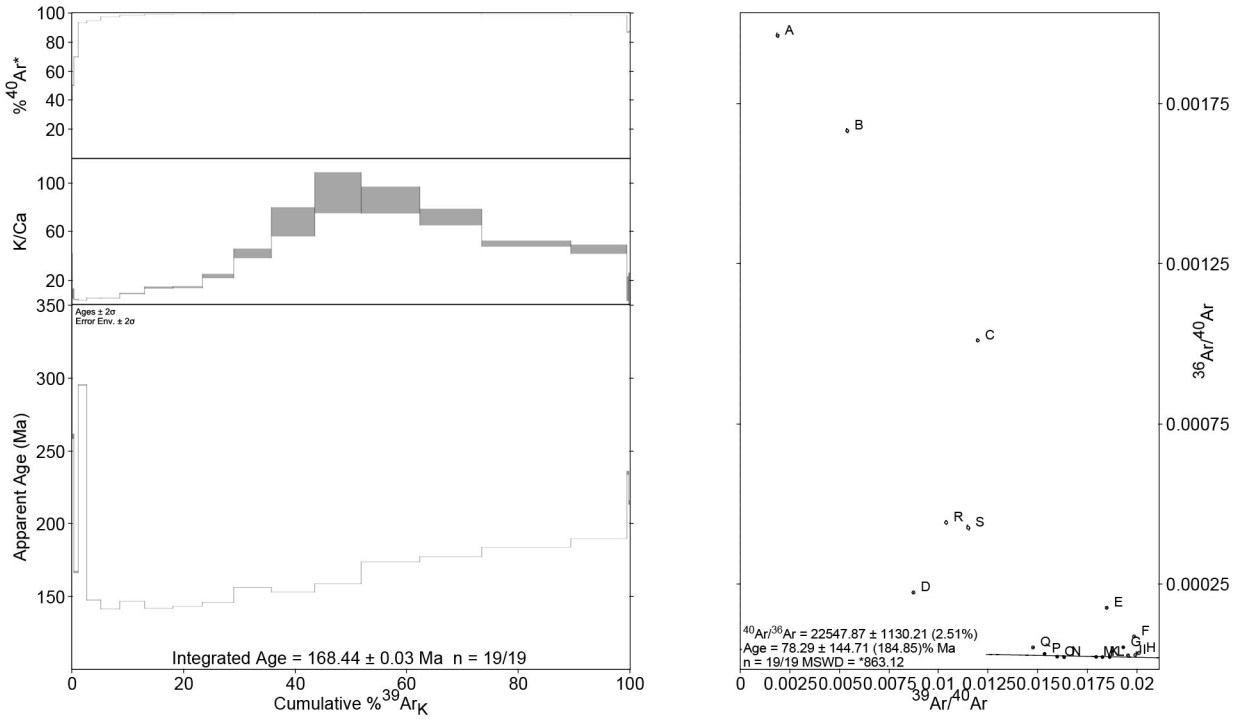

Figure A26. Age spectrum and inverse isochron plots for white mica sample 24RN287 #1.

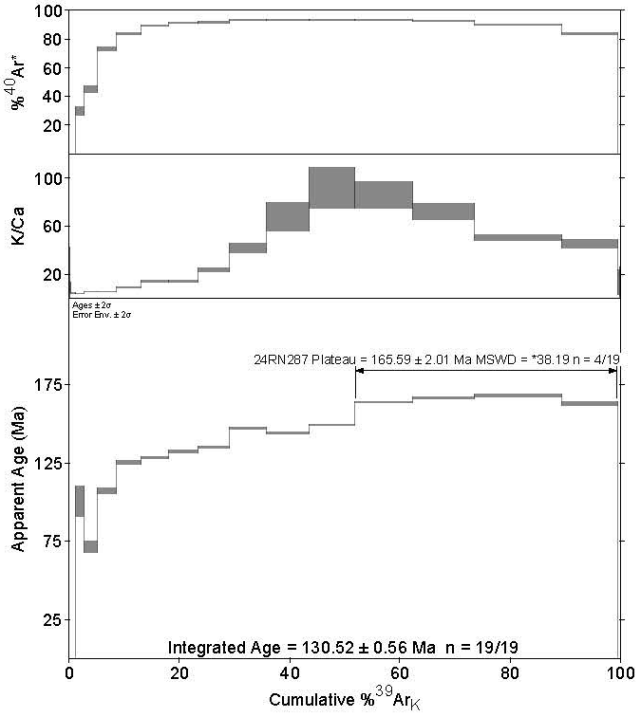

Figure A27. Recalculated age spectrum for white mica sample 24RN287 #1 using the initial $^{40}Ar/^{36}Ar$ ratio from the inverse isochron plot instead of the typical atmospheric $^{40}Ar/^{36}Ar$ ratio.

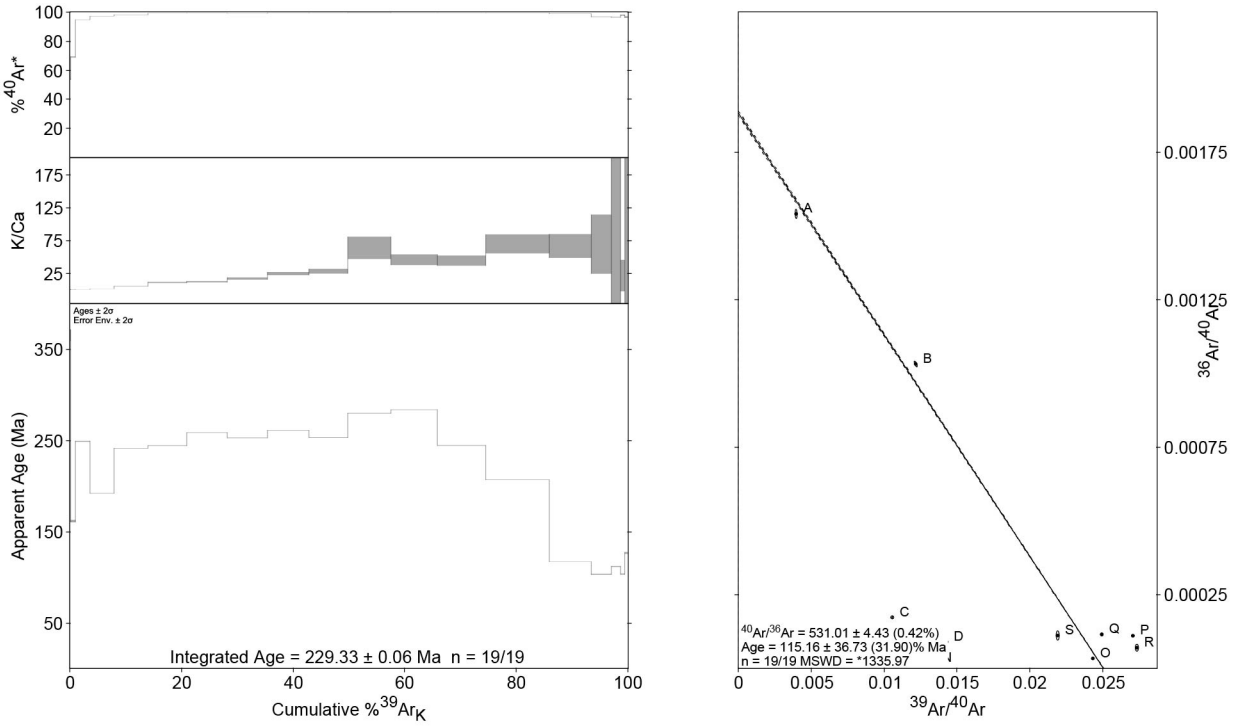

Figure A28. Age spectrum and inverse isochron plots for white mica sample 24RN287 #2.

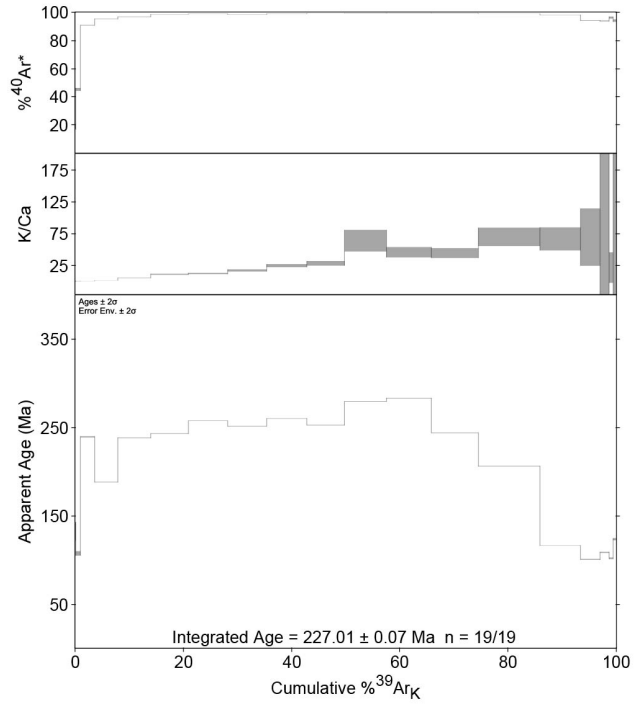

Figure A29. Recalculated age spectrum for white mica sample 24RN287 #2 using the initial $^{40}Ar/^{36}Ar$ ratio from the inverse isochron plot instead of the typical atmospheric $^{40}Ar/^{36}Ar$ ratio.

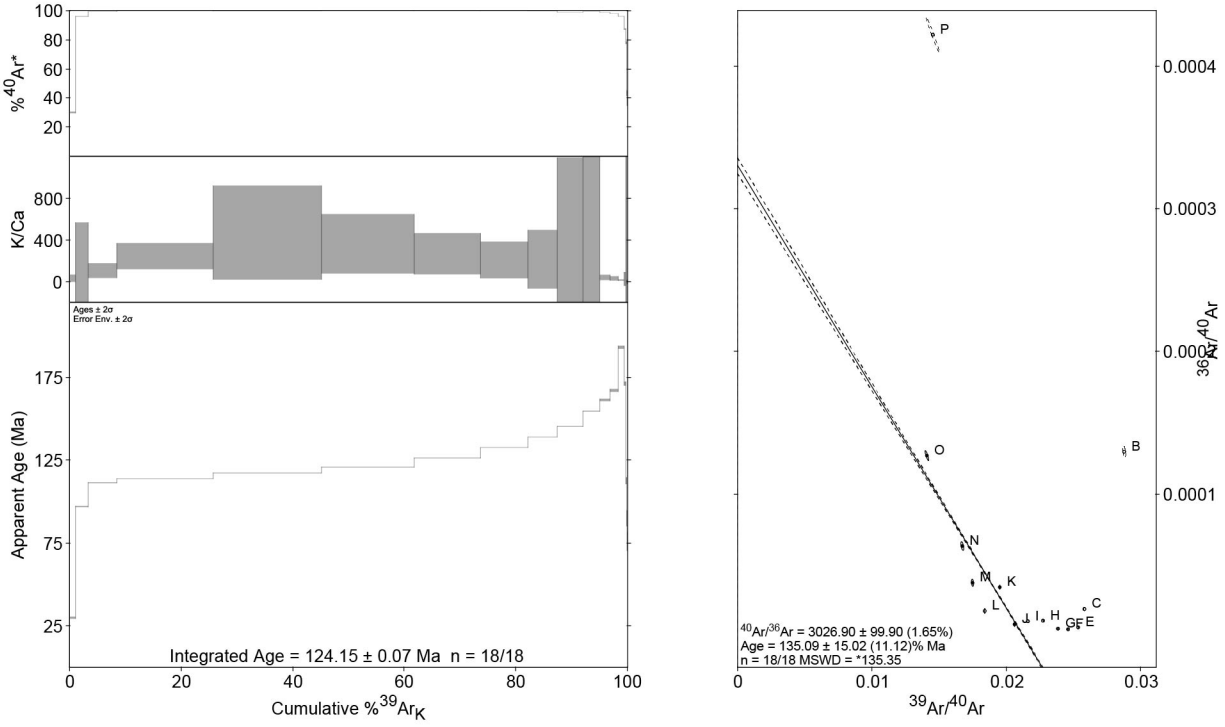

Figure A30. Age spectrum and inverse isochron plots for white mica sample 24RN465 #1.

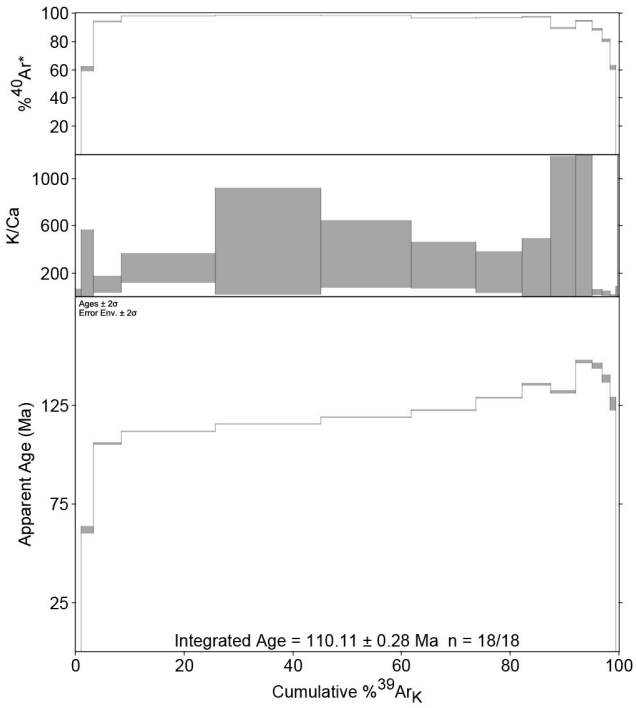

Figure A31. Recalculated age spectrum for white mica sample 24RN465 #1 using the initial 40Ar/36Ar ratio from the inverse isochron plot instead of the typical atmospheric 40Ar/36Ar ratio.

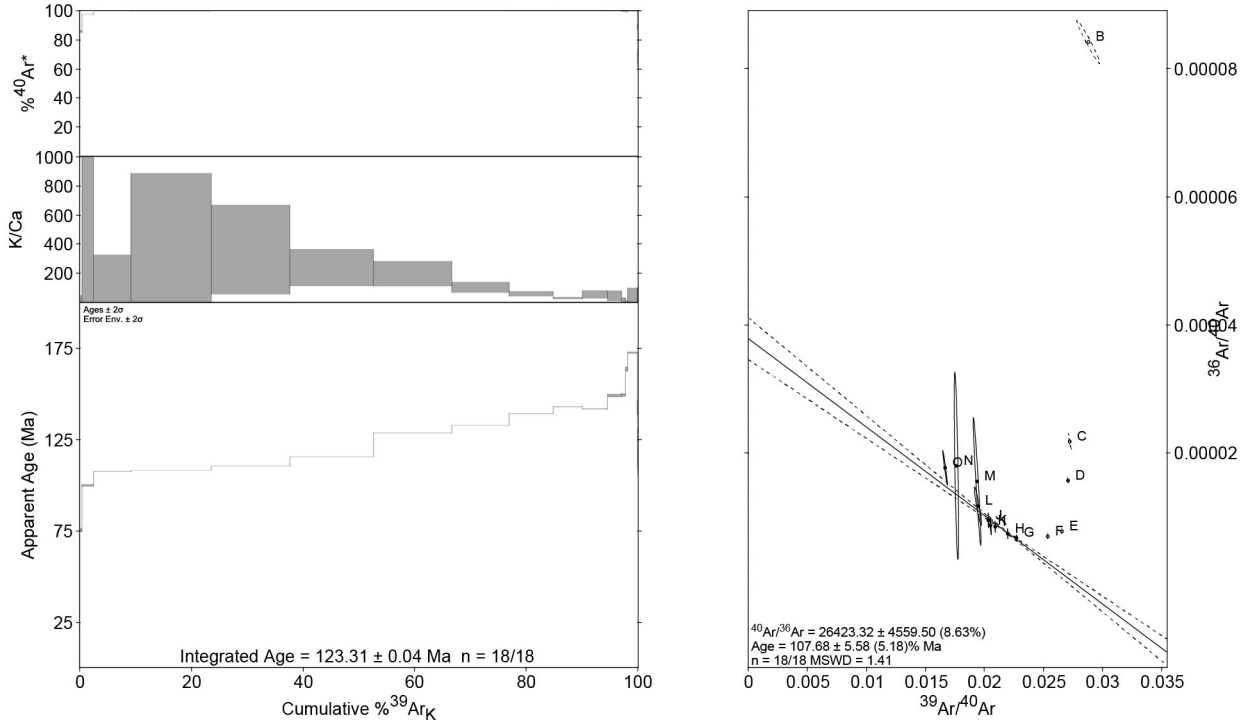

Figure A32. Age spectrum and inverse isochron plots for white mica sample 24RN465 #2.

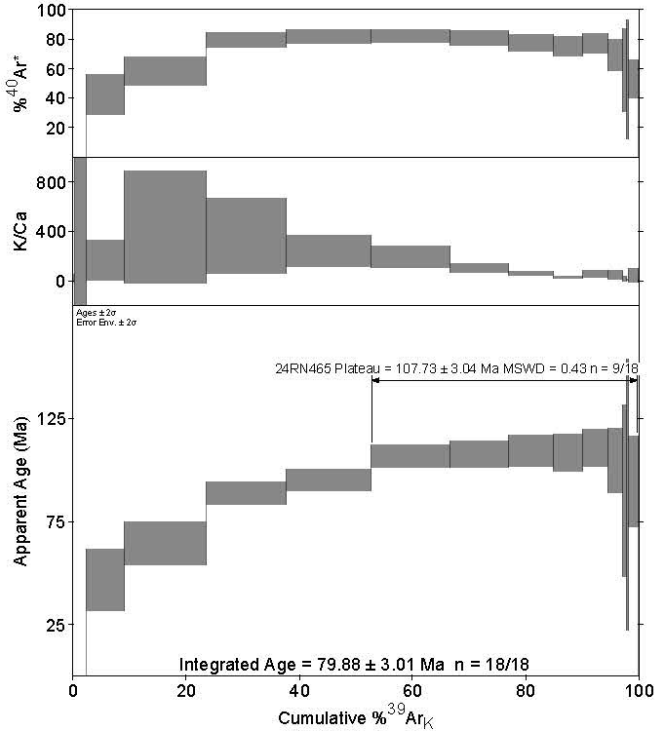

Figure A33. Recalculated age spectrum for white mica sample 24RN465 #2 using initial $^{40}Ar/^{36}Ar$ ratio from the inverse isochron plot instead of typical atmospheric $^{40}Ar/^{36}Ar$ ratio.

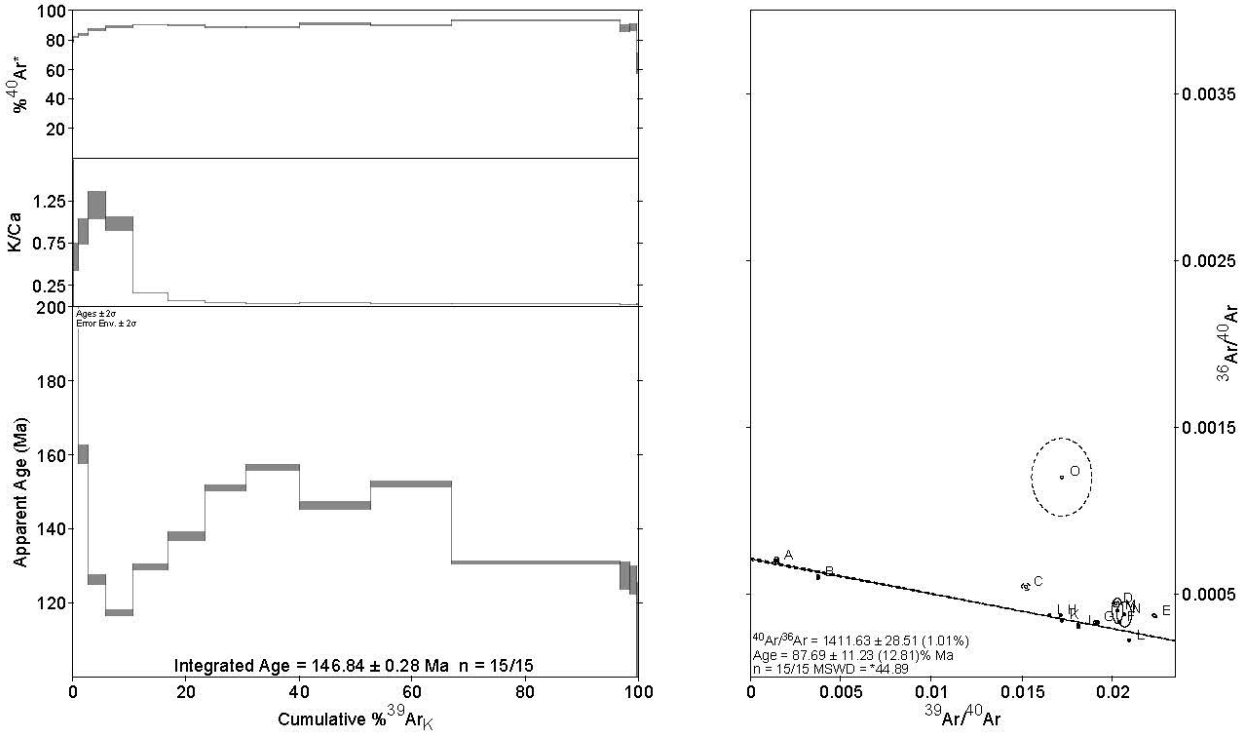

Figure A34. Age spectrum and inverse isochron plots for hornblende sample 24TJN141.

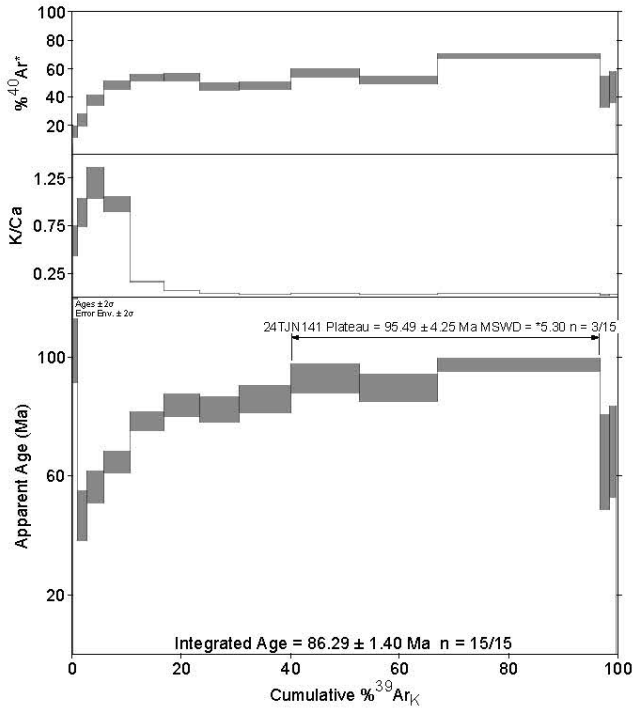

Figure A35. Recalculated age spectrum for hornblende sample 24TJN141 using the initial $^{40}Ar/^{36}Ar$ ratio from the inverse isochron plot instead of the typical atmospheric $^{40}Ar/^{36}Ar$ ratio.

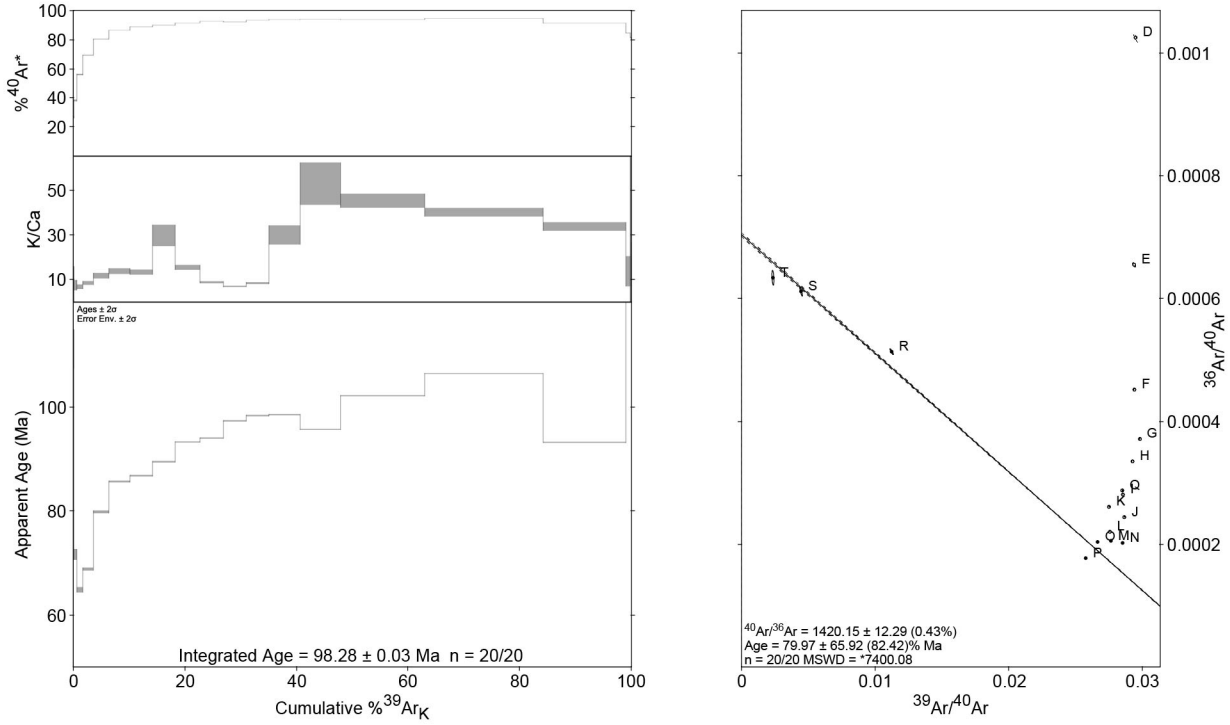

Figure A36. Age spectrum and inverse isochron plots for white mica sample 24TJN212.

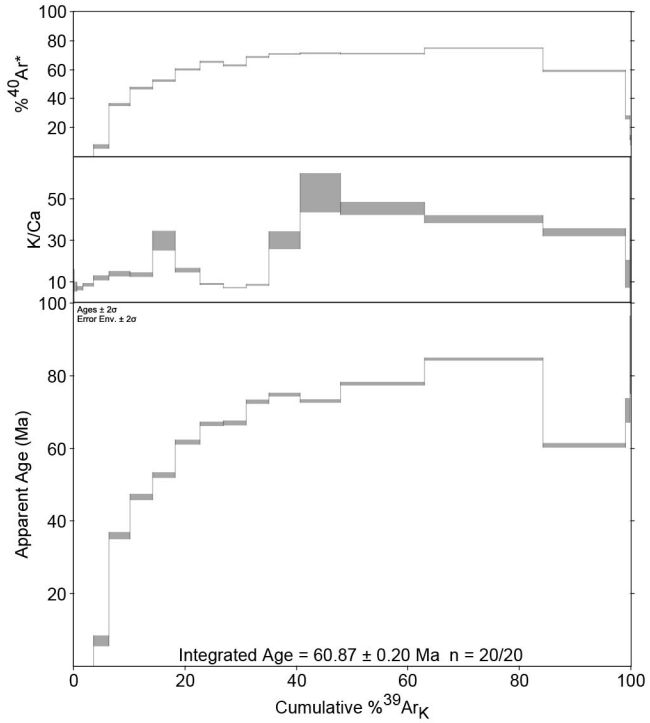

Figure A37. Recalculated age spectrum for white mica sample 24TJN212 using the initial $^{40}Ar/^{36}Ar$ ratio from the inverse isochron plot instead of the typical atmospheric $^{40}Ar/^{36}Ar$ ratio.

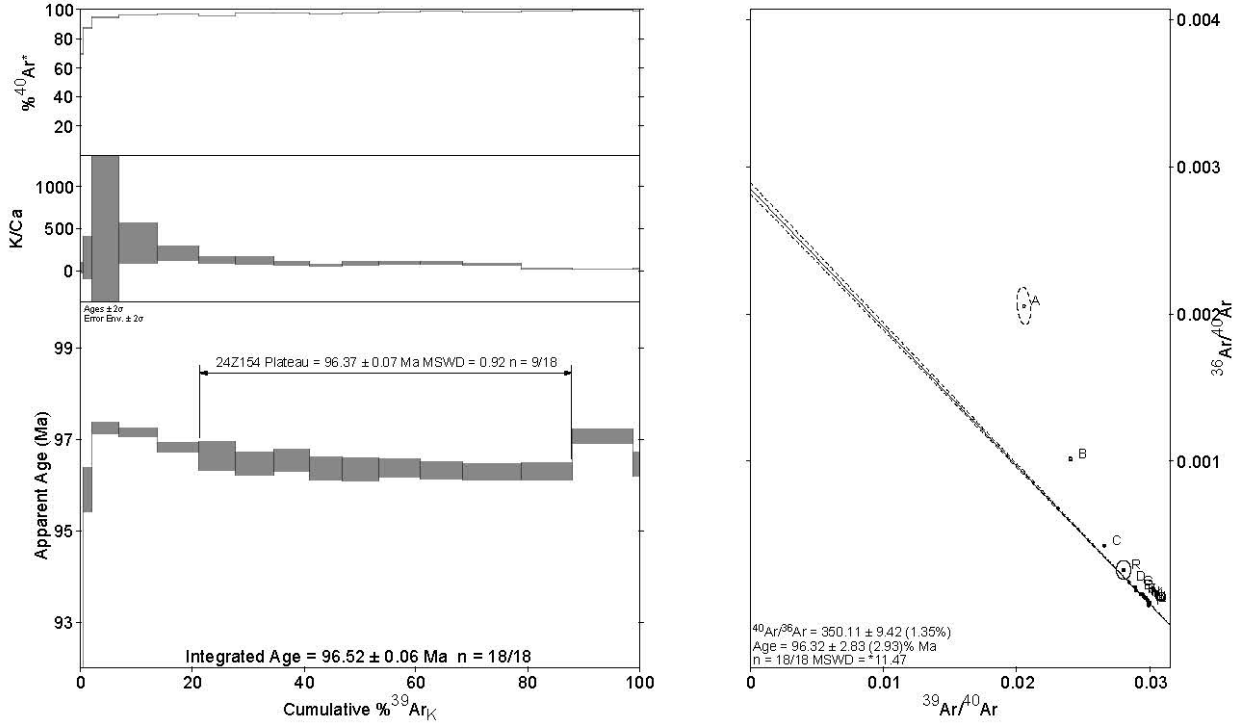

Figure A38. Age spectrum and inverse isochron plots for muscovite sample 24Z154.

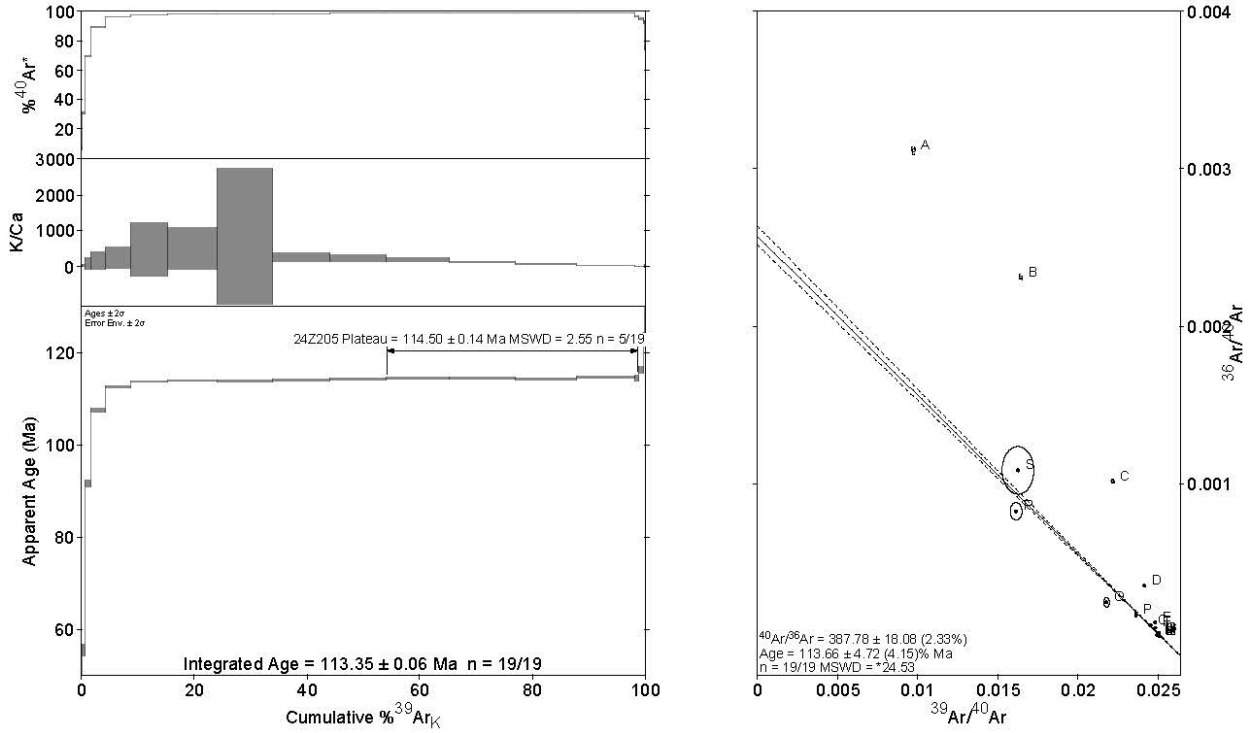

Figure A39. Age spectrum and inverse isochron plots for biotite sample 24Z205.

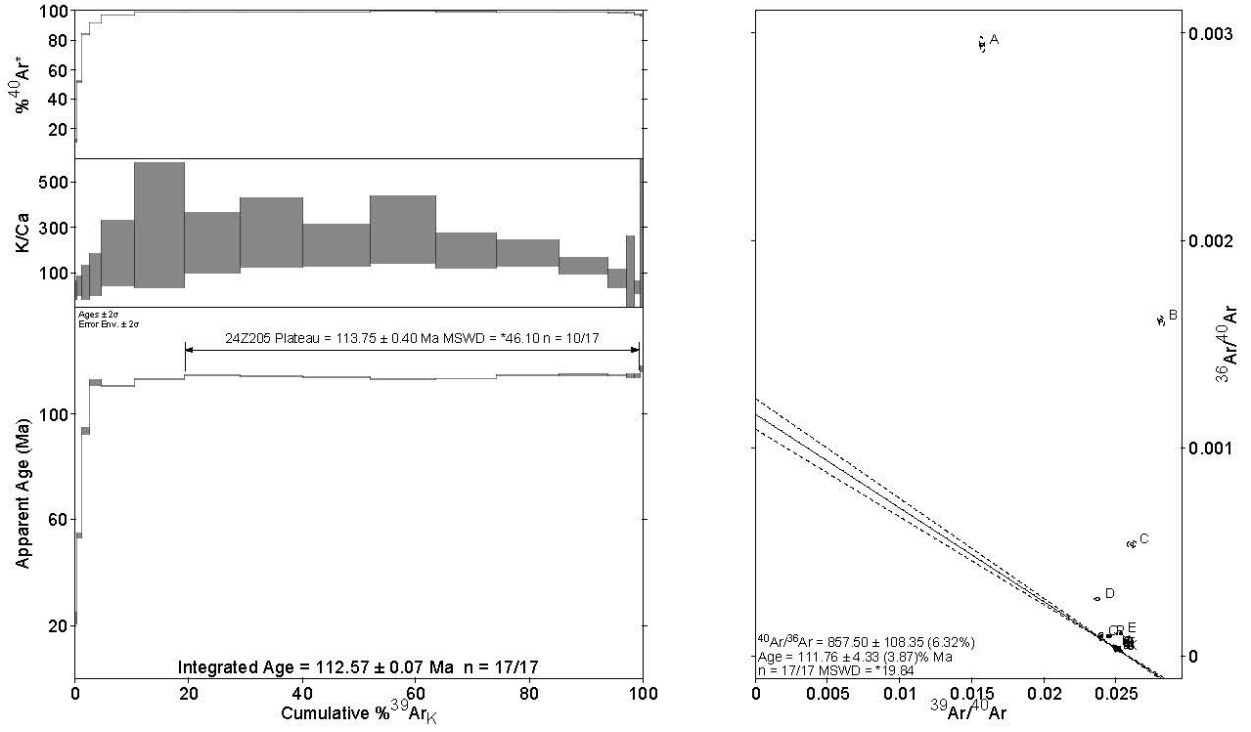

Figure A40. Age spectrum and inverse isochron plots for white mica sample 24Z205.

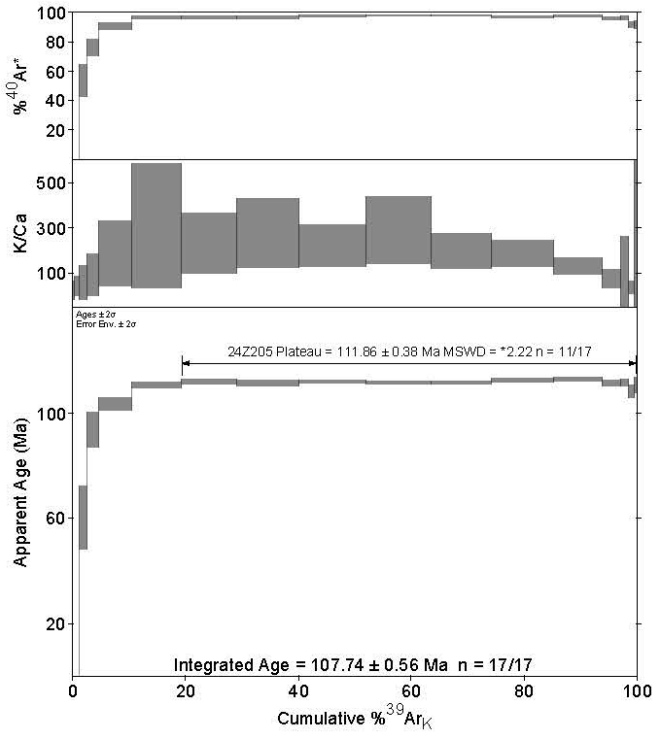

Figure A41. Recalculated age spectrum for white mica sample 24Z205 using the initial $^{40}Ar/^{36}Ar$ ratio from the inverse isochron plot instead of the typical atmospheric $^{40}Ar/^{36}Ar$ ratio.

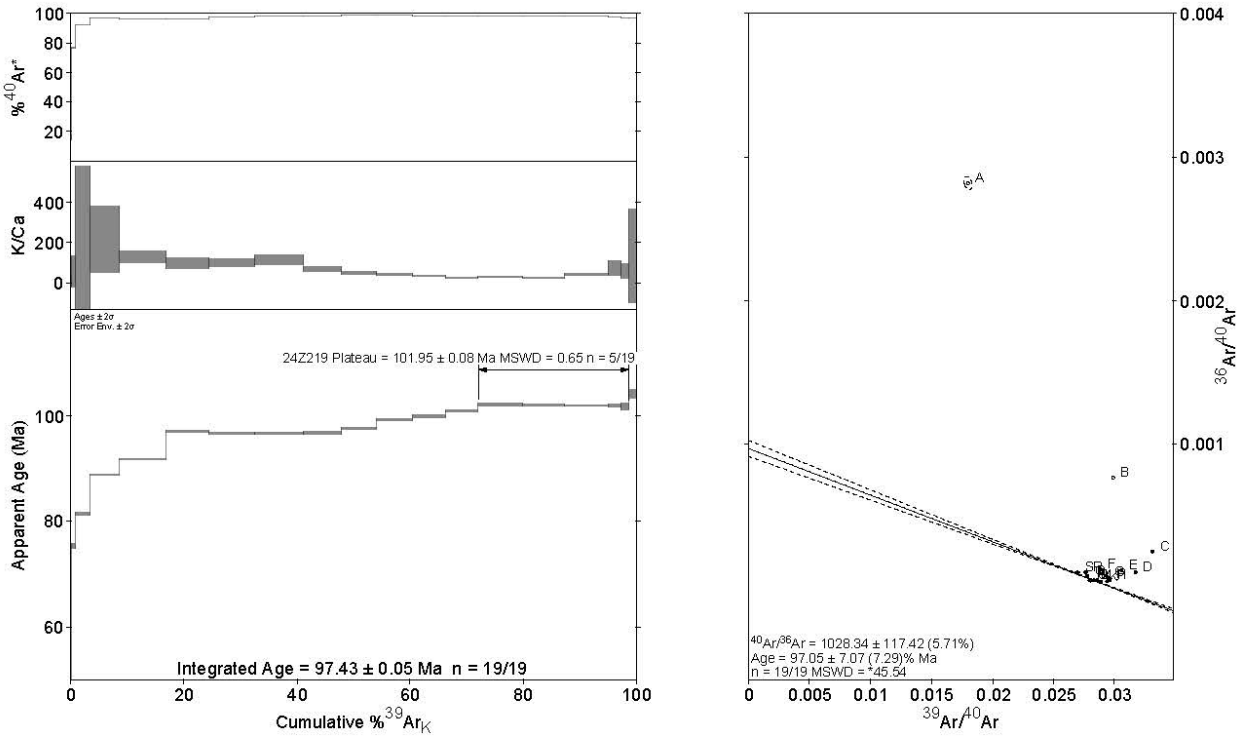

Figure A42. Age spectrum and inverse isochron plots for white mica sample 24Z219.

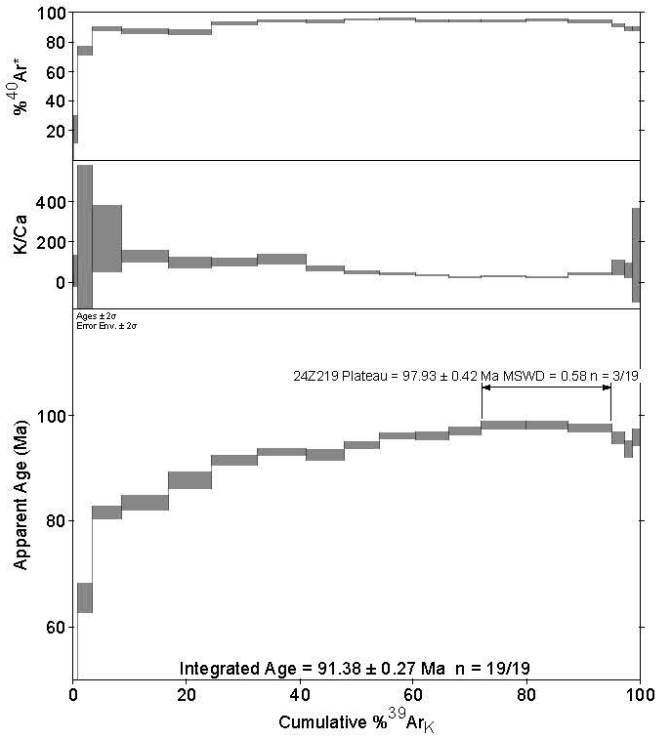

Figure A43. Recalculated age spectrum for white mica sample 24Z219 using the initial 40Ar/36Ar ratio from the inverse isochron plot instead of the typical atmospheric 40Ar/36Ar ratio.

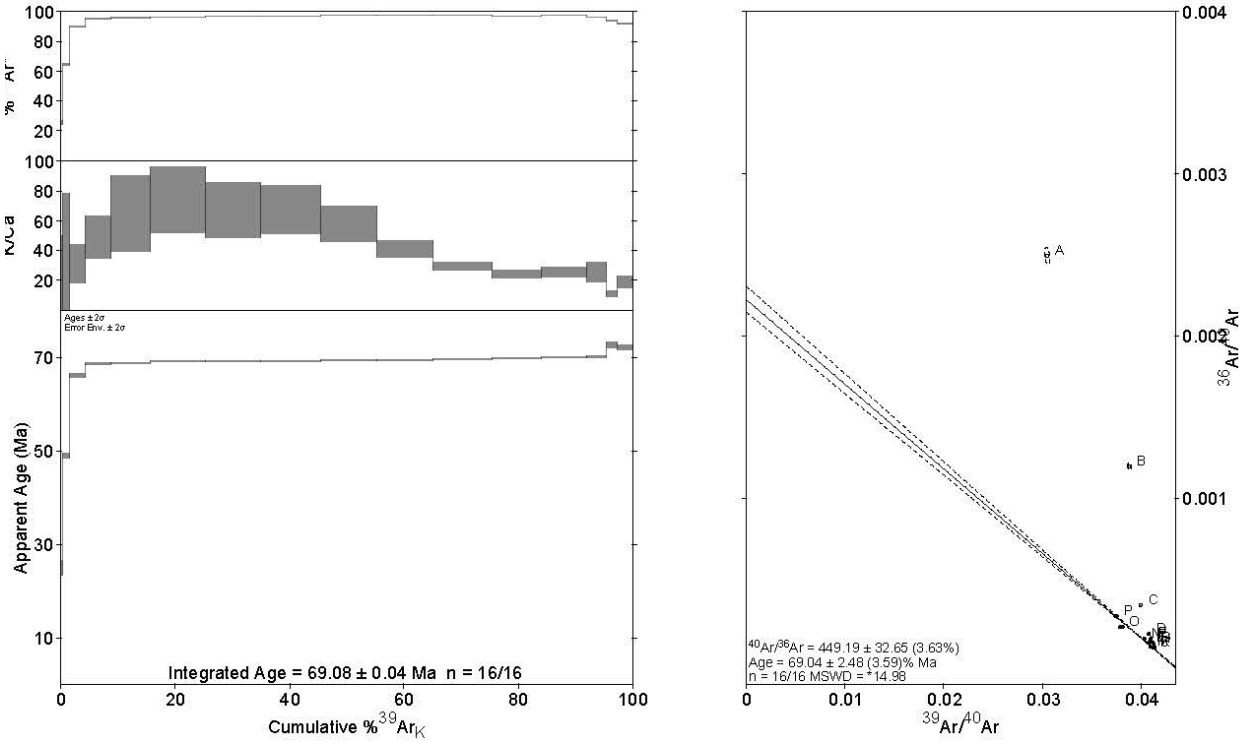

Figure A44. Age spectrum and inverse isochron plots for muscovite sample 24Z261.

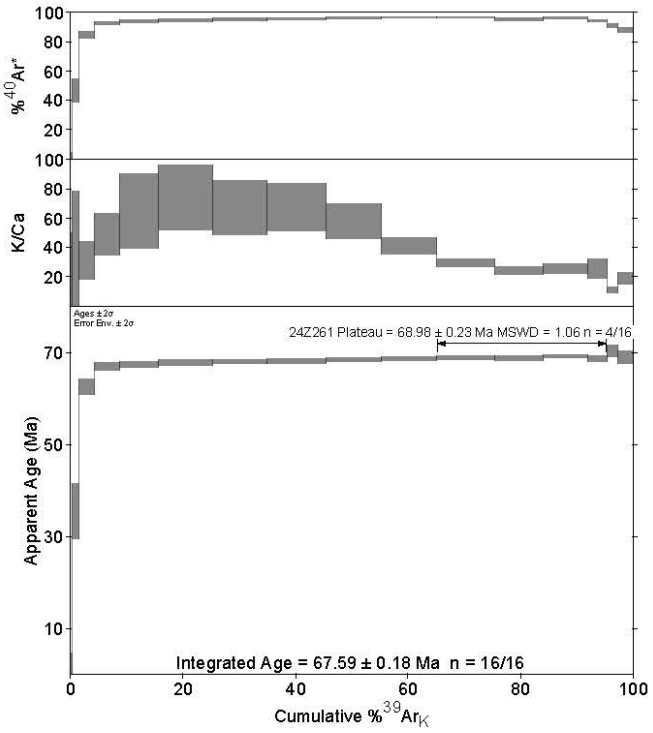

Figure A45. Recalculated age spectrum for muscovite sample 24Z261 using the initial $^{40}Ar/^{36}Ar$ ratio from the inverse isochron plot instead of the typical atmospheric $^{40}Ar/^{36}Ar$ ratio.